TRACE ELEMENTAL ANALYSIS OF SELENIUM AND ANTIMONY USING HYDRIDE GENERATION COUPLED TO LASER INDUCED BREAKDOWN SPECTROSCOPY

By

Latresa J. Williamson

Submitted in Partial Fulfillment of the Requirements for the Degree of
Master of Science in the Chemistry Program

YOUNGSTOWN STATE UNIVERSITY
AUGUST 2010

TRACE ELEMENTAL ANALYSIS OF SELENIUM AND ANTIMONY USING HYDRIDE GENERATION COUPLED TO LASER INDUCED BREAKDOWN SPECTROSCOPY

Latresa J. Williamson

Signature:

_____

Latresa J. Williamson, Student Date

Approvals: _____

Dr. Josef Simeonsson Date
Thesis Advisor

_____

Dr. Peter Norris Date
Committee Member

_____

Dr. Daryl Mincey Date
Committee Member

_____

Peter J. Kasvinsky Date
Dean of School of Graduate Studies and Research

ABSTRACT

Detection of metalloids such as selenium and antimony in the environment is important for technological and health reasons. Selenium in trace amounts has biological importance and hydride generation is one of the most effective sample introduction techniques for analytical atomic spectroscopy measurements. Aqueous solutions of selenium and antimony are converted to a gaseous form via hydride generation and the gas is delivered to an atomizer for measurement. Laser Induced Breakdown Spectroscopy, LIBS, is the atomic emission spectroscopy method that is used in this research to measure the gaseous form of the analyte generated by the hydride approach. Analyte atoms are atomized and excited by a laser-produced plasma and the atomic emission is measured at an element-specific wavelength. Optimization of the instrument to obtain the maximum wavelength of emission was performed using a 10 ppm solution of each element. The optimized parameters were used to measure various concentrations of each element in solution ranging from 0 to 10 ppm. A calibration curve was generated using the wavelength to plot intensity as a function of concentration. A limit of detection, LOD, was determined using the data from the calibration curve. Additional research in this work included studying the characteristics and properties of laser produced-plasmas and determining how this information can be utilized in further studies of trace analysis of selenium and antimony.

ACKNOWLEDGEMENTS

I'd like to thank the Almighty God for the many blessings He has bestowed upon me. I'd like to thank my advisor, Dr. Simeonsson, for all of his guidance, patience, and understanding. I'd like to thank the YSU Chemistry Department and Graduate School and I'd like to offer a special thanks to Dr. Wagner because without his help I would not have made it into the M.S. Program; he went the extra mile just for me and helped me get through special circumstances with the proper paperwork! Thank you to my committee members, Dr. Norris and Dr. Mincey. I'd like to thank my employer, The Gebauer Company, for making it possible for me to attend school while still working full time and for the support and encouragement of the executive group, my supervisors, and my co-workers.

I'd like to thank my family for the love, respect, encouragement, and support they have given me throughout my life. I'd like to thank my family for making me feel proud even when I didn't think I could make it. Thanks to my parents for making me feel special and always knowing I would be successful. My ***entire*** family has always made me feel like a hero! Thanks to my children DeWyon and JeLaya for your understanding and support through the many years of my schooling. I'd like to thank my church family for all of their prayers and support. I'd like to dedicate this thesis to my Aunt and Uncle, Roosevelt and Vanessa Haynes, because they played an important role in my life and helped to raise me. I'd like to dedicate this thesis to my Grandmother, the late Mrs. Eunice Hosey, she would've been very proud! I'd also like to dedicate this thesis to my Grandfather, Frank Smith, who is and always will be my hero!

TABLE OF CONTENTS

TITLE PAGE ……i

SIGNATURE PAGE ……ii

ABSTRACT ……iii

ACKNOWLEDGEMENTS ……iv

TABLE OF CONTENTS ……..v-vii

LIST OF FIGURES ……...viii-x

LIST OF TABLES ……xi-xii

LIST OF ABBREVIATIONS AND SYMBOLS ……...xiii-xv

CHAPTER 1: INTRODUCTION ……1-13

1.1 ATOMIC EMISSION SPECTROSCOPY, AES ……...1

1.1.1 Flame-AES ……4

1.1.2 Inductively Coupled Plasma-AES, ICP-AES ……4

1.1.3 Laser-Produced Plasma-AES ……..6

1.1.3.1 Plasma Decay and Electron Density ……7

1.1.4 Laser Induced Breakdown Spectroscopy, LIBS ……8

1.1.5 Comparison of AES Techniques ……..8

1.2 DETECTOR SYSTEM ……...10

CHAPTER 2: SELENIUM AND ANTIMONY ……..……14-16

2.1 SELENIUM ……....14

2.2 ANTIMONY ……15

CHAPTER 3: GOAL OF THE PROJECT ……..……17

CHAPTER 4: EXPERIMENTAL ……..……..18-20

4.1 HYDRIDE GENERATION-LASER INDUCED BREAKDOWN SPECTROSCOPY, HG-LIBS ……..……18

4.1.1 Peristaltic Pump …….…..…19

4.2 LASER SYSTEM …….……..20

CHAPTER 5: MATERIALS AND METHODS …….…..….21-23

5.1 REAGENTS AND STANDARDS …….……21

5.2 PROCEDURE: HG-LIBS ……..……21

5.2.1 Emission Peak ……..……..……..22

5.2.2 Generation of a Calibration Curve ……...23

CHAPTER 6: RESULTS AND DISCUSSION ……24-71

6.1 HYDROGEN EMISSION SPECTRA ……24

6.1.1 Stark Broadening and Electron Density of Hydrogen Emission Peaks…… 29

6.1.1.1 Plasma Diagnostics …….33

6.1.2 Discussion ……37

6.2 ANTIMONY EMISSION SPECTRA ……39

6.2.1 Determination of Plasma Excitation Temperature for Antimony……..46

6.2.2 Antimony Calibration Curves……...52

6.2.3 Discussion ……57

6.3 SELENIUM EMISSION SPECTRA ……60

6.3.1 Selenium Calibration Curves ……64

6.3.2 Discussion ……67

6.4 CONCLUSION ……...70

6.5 FUTURE WORK ……71

7.0 REFERENCES ……..72-73

LIST OF FIGURES

Figure 1: Atomic Emission Spectroscopy ...……...1

Figure 2: Boltzmann Distribution ……...……...3

Figure 3: Schematic of an ICP Torch ……...……..……6

Figure 4: Detector System ……..……..13

Figure 5: Hydride Generator Apparatus ..……20

Figure 6: Nd: Yag Laser System ……..……20

Figure 7: Hydrogen Emission Peak – 1..…….....25

Figure 8: Hydrogen Emission Peak - 2 ..…….……27

Figure 9: Hydrogen Emission Peak - 3……..…….....27

Figure 10: Hydrogen Emission Peak - 4 ..…….…….…….....28

Figure 11: Hydrogen Emission Peak - 5……...28

Figure 12: Hydrogen Emission Peak - 6.……..……29

Figure 13: Hydrogen Emission Peaks: Different Time Delays-1……..30

Figure 14: Hydrogen Emission Peaks: Different Time Delays-2 ……30

Figure 15: Hydrogen Emission Peaks: Different Time Delays-3 ……31

Figure 16: Hydrogen Emission Peaks: Different Time Delays-4 ……32

Figure 17: Hydrogen Emission Peaks: Different Time Delays and ND Filter……..32

Figure 18: FWHM Peak Width V. Plasma Decay Time for Hydrogen ..…..35

Figure 19: Electron Density V. Plasma Decay Time for Lower and Higher Energy of Hydrogen Emission Peaks ……...36

Figure 20: Sb Emission Peak at 259.9 nm ……...40

Figure 21: Sb Emission Peak at 252.9 nm ……...41

Figure 22: Sb Emission Peak at 259.9 nm, Different Time Delays …….41

Figure 23: Sb Emission Peak at 252.9 nm, Different Time Delays …….42

Figure 24: Sb Emission Peak at 259.9 nm, Different Time Delay, 100 ns gate, Low Laser Energy ……43

Figure 25: Sb Emission Peak at 252.9 nm, Different Time Delay, 100 ns gate, Low Laser Energy ……..44

Figure 26: Sb Emission Peak at 259.9 nm, Different Time Delay, 100 ns gate, High Laser Energy ……..45

Figure 27: Sb Emission Peak at 252.9 nm, Different Time Delay, 100 ns gate, High Laser Energy ……45

Figure 28: Sb Emission Peak Intensity V. Plasma Decay Time at Low Laser Energy……49

Figure 29: Sb Emission Peak Area V. Plasma Decay Time at Low Laser Energy ……..50

Figure 30: Sb Emission Peak Intensity V. Plasma Decay Time at High LaserEnergy……..50

Figure 31: Sb Calibration Curve-1, 252.9 nm ……..54

Figure 32: Sb Calibration Curve-1, 259.9 nm ……..54

Figure 33: Sb Calibration Curve-2, 252.9 nm……...55

Figure 34: Sb Calibration Curve-2, 259.9 nm ……55

Figure 35: Sb Calibration Curve-3, 252.9 nm…….56

Figure 36: Sb Calibration Curve-3, 259.9 nm ……56

Figure 37: Sb Calibration Curve, 259.9 nm, Higher Laser Energy ……57

Figure 38: Se Emission Peak – 1 ……60

Figure 39: Se Emission Peaks at Different Slit Widths ……..62

Figure 40: Se Emission Peaks at Different Time Delays-1…….62

Figure 41: Se Emission Peaks at Different Time Delays-2 ……63

Figure 42: Se Emission Peaks at Different Time Delays-3 ……63

Figure 43: Se Emission Peaks at Different Time Delays-4 ……64

Figure 44: Se Calibration Curve-1 ……..65

Figure 45: Se Calibration Curve-2 ……..66

Figure 46: Se Calibration Curve-3 ……..66

Figure 47: Se Calibration Curve-4 ……..67

LIST OF TABLES

TABLE 1: Comparison of AES Techniques ……10

TABLE 2: Instrument Parameters for Hydrogen Emission Peaks ……...25

TABLE 3: Constant Instrument Parameters and Conditions ……...26

TABLE 4: Instrument Parameters for Figures 8-12 ……26

TABLE 5: FWHM Data for Lower Energy Hydrogen Emission Peaks …..34

TABLE 6: FWHM Data for Higher Energy Hydrogen Emission Peaks ….34

TABLE 7: Time Delay and Electron Density for Lower Laser Energy …...35

TABLE 8: Time Delay and Electron Density for Higher Laser Energy …..36

TABLE 9: Calculated Electron Densities ……39

TABLE 10: Instrument Parameters for Sb at 252.9 nm and 259.9 nm ……43

TABLE 11: Sb Emission Peak Intensity/Area V. Time Delay for 252-254 nm at Low Laser Energy ……..46

TABLE 12: Sb Emission Peak Intensity/Area V. Time Delay for 259-261 nm at Low Laser Energy ……..47

TABLE 13: Plasma Temperature Calculations Using Peak Intensity at Low Laser Energy ……...48

TABLE 14: Plasma Temperature Calculations Using Peak Area at Low Laser Energy ……...49

TABLE 15: Sb Emission Peak Intensity and Time Delay for 252-254 nm at High Laser Energy ……...51

TABLE 16: Sb Emission Peak Intensity and Time Delay for 259-261 nm at High Laser Energy ……...52

TABLE 17: Plasma Temperature Calculations Using Peak Intensity at High Laser Energy ……..……..52

TABLE 18: Plasma Temperature Comparisons ……..59

TABLE 19: Sb Detection Limit Comparisons …….59

TABLE 20: Instrument Parameters and Conditions for Se Emission Peaks 61

TABLE 21: Comparison of HG-LIBS LOD Values ……69

LIST OF ABBREVIATIONS AND SYMBOLS

AES ……...Atomic Emission Spectroscopy

LASER ……..Light Amplification by Stimulated Emission of Radiation

HG ……Hydride Generation

LIBS ……Laser Induced Breakdown Spectroscopy

ICP-AES ……..Inductively Coupled Plasma Atomic Emission Spectroscopy

HPLC ……..High Performance Liquid Chromatography

PMT ……Photomultiplier Tube

Se ……...Selenium

Sb ……Antimony

Sn ……Tin

Ar ……Argon

H_2 ……...Hydrogen

$NaBH_4$ ……Sodium Borohydride

HCl ……Hydrochloric Acid

LOD ……Limit of Detection

NaCl ……Sodium Chloride

SD ……Standard Deviation

mL ……Milliliter

µs ……Microsecond

ns ……Nanosecond

µm ……Micrometer

m/v ……Mass per volume

v/v ……Volume per volume

V ……Volts

mV ……Millivolts

Hz ……Hertz

K ……Kelvin

°C ……..Degree Celsius

% ……Percentage

sccm ……Standard cubic centimeters per minute

σ ……Standard Deviation

a.u. ……Arbitrary units

t_d ……Time delay

t_w ……..Time (gate) width

N.D. ……Neutral Density

ppm ……Parts per million

ppb ……...Parts per billion

ppt ……...Parts per trillion

UV/VIS ……Ultraviolet-Visible Spectroscopy

mg/kg ……Milligrams per kilogram

ng/kg ……Nanograms per kilogram

U.S. EPA ……..United States Environmental Protection Agency

µg/L ……Microgram per liter

µg/dL ……..Microgram per deciliter

Avg ……..Averaging

r.p.m. ……Revolutions per minute

mL/min ……...Milliliters per minute

nm/min ……Nanometers per minute

Nd: YAG ……..Neodymium-doped yttrium aluminum garnet

FWHM …….full width half maximum

J ……Joules

Å……angstroms

mJ……millijoules

Te…….Tellurium

As……Arsenic

CHAPTER 1: INTRODUCTION

1.1 ATOMIC EMISSION SPECTROSCOPY, AES

Atomic Emission Spectroscopy, AES, is the measurement of light emissions from excited atoms. The concentration of an analyte/element can be determined from the quantitative measurement of these emissions. A source such as a plasma, flame, or discharge is used to provide the energy to atomize and excite analyte atoms and promote them to higher energy levels. The optical emission corresponds to the excited atoms returning to lower energy level(s) and emitting light that is detected by a photon detector system. Figure 1 shows a diagram of the process of AES.

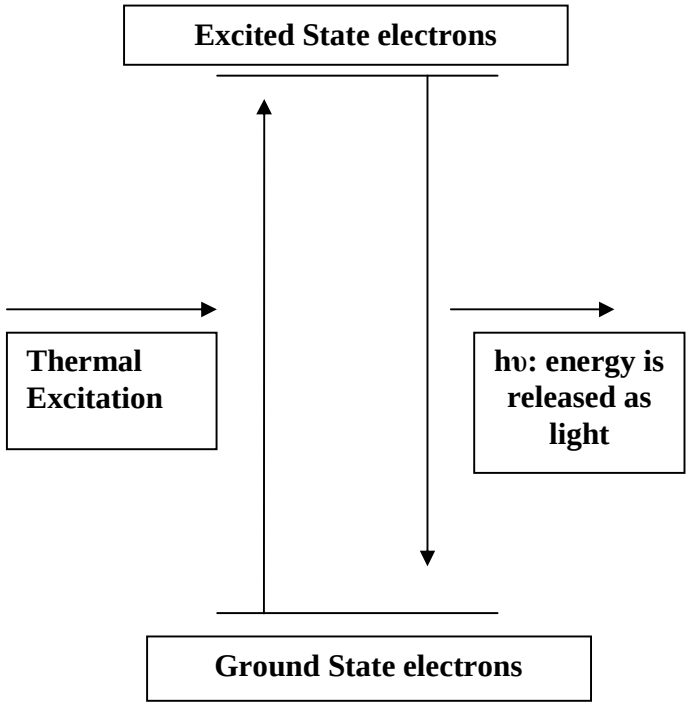

Figure 1. Schematic representation of Atomic Emission Spectroscopy

In AES, the process begins with sample introduction. Sample introduction techniques vary with AES but the usual procedure for liquid samples is to aspirate the sample solution and convert it into an aerosol to introduce small droplets of the analyte into the atomizer. This sample introduction method helps prevent the atomizer from being extinguished or from incompletely removing solvent. The heat of the atomizer desolvates or removes excess solvent/water from the sample droplets through volatilization and evaporation processes and dries the sample particles.[1] In atomization, chemical bonds are broken and free atoms are produced. These free atoms become excited and gain energy from collisions in the atomizer. The atoms leave the ground state and are promoted to an excited state where they emit light upon returning to lower energy levels. The excited atoms return to lower energy states and eventually to the ground state due to the loss of energy. The relationship that exists between atoms in an excited state and atoms in a lower state is based on the Boltzmann equilibrium.[2] The Boltzmann equilibrium is described in the following expression:

Boltzmann Equation: $N_1/N_0 = e^{-\Delta E/kT}$

N_1 = number of atoms in the upper state

N_0 = number of atoms in the lower state

ΔE = energy difference between upper and lower states, cm^{-1}

k = Boltzmann constant, J/K

T = absolute temperature, K

For degeneracy as in figure 2, the equation is:

$N_1/N_0 = [g_1/g_0]\, e^{-\Delta E/kT}$

Temperature has a significant effect on the population of atoms in an energy level. Atoms in the excited state and atoms in the ground state exist in a certain ratio when thermal equilibrium occurs. The Boltzmann equation assumes that energy levels are thermally populated and that the system is in thermal equilibrium. Temperature variation must be controlled in AES for reproducible data or results.[3] The elemental composition of a sample can be determined by evaluating the spectrum of the emitted light of excited atoms in an atomizer cell.[2] Every element has a characteristic emission spectrum that is related to its electronic structure. For analysis, a range of different wavelengths is used to determine the identity of multiple elements in a solution or one wavelength for single element analysis. For single element analysis, a narrow range is selected to maximize the sensitivity and selectivity of measurements of a particular element.

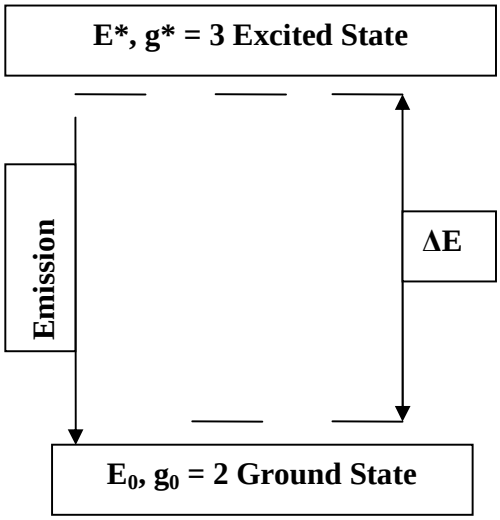

Figure 2. Boltzmann Distribution

Two energy levels (E) with different degeneracies (g). Ground state atoms can be promoted to the excited state and excited state atoms can emit light and return to the ground state

Some common AES excitation sources are *Flame, Inductively Coupled Plasma (ICP), Spark and Arc, Laser-Produced Plasmas,* and *Microwave-Induced Plasma*.[4] These excitation sources use different approaches for exciting free atoms. The excitation source and the atomizer can be the same in AES. Effective methods and techniques in AES utilize atomizers that completely remove the sample from its matrix and completely atomize all elements. The excitation source should have enough thermal energy to completely excite all elements and be able to handle a range of solvents, solids, liquids and gases.

1.1.1 Flame-AES

In flame atomic emission spectroscopy, a flame is used as both the atomizer and excitation source. The flame technique generally uses a total consumption burner that aspirates the sample solution directly into the flame.[1] The heat of the flame desolvates the sample aerosol and creates free atoms. The heat of the flame along with free atom collisions excites the free atoms and promotes them to higher energy states. The temperature of the flame is on average < 3000 K and is lower than many other atomizers. Alkali and alkaline earth metals are usually analyzed by this technique due to their low atomization temperatures.[2] Sample introduction in Flame-AES is often an issue. Approximately 85% of the sample is lost during sample introduction and only 15% of the sample is atomized and excited. Flame AES is useful for single element analysis and elements that become excited at low temperatures.[1]

1.1.2 Inductively Coupled Plasma-AES

ICP atomic emission spectroscopy utilizes a plasma as the atomization and excitation source. A plasma is an electrically neutral, partially ionized gas made up of ions, electrons, and atoms.[1] Plasmas are characterized by their electron density and temperature. The temperature of a plasma in ICP-AES usually ranges from 4000-8000 K. Plasmas in AES acquire their energy from an electric or magnetic field and this energy must be maintained for the plasma to be used for AES. In ICP-AES, the energy is acquired from electrical currents produced by electromagnetic induction.[4] Plasmas and their properties will be discussed in further detail in the section of *Laser-Produced Plasma*-AES. In ICP-AES, the stable, high temperature plasma is formed by an ICP torch. The ICP is a continuous plasma meaning it does not form and quickly decay. The density and temperature of the plasma decrease from the core of the plasma outward.

The ICP torch is made of three concentric tubes and is partially enclosed by a water-cooled coil that is powered by a radio frequency generator.[4] The field becomes magnetically activated when the power is turned on and an inert gas such as Argon flows through the torch. The flowing gas becomes electrically conductive when a tesla coil ignites the gas and a plasma is formed.[4] A diagram in figure 3 shows the details of an ICP torch. In ICP-AES, the sample is introduced (solid, liquid, or gas) directly inside the plasma and atomization and excitation occur as previously discussed in Flame-AES. An advantage of ICP-AES is the sensitivity of the technique due to the high temperature plasma source. This sensitivity results in good emission spectra for most elements. Applications of ICP-AES include multi-elemental analysis.

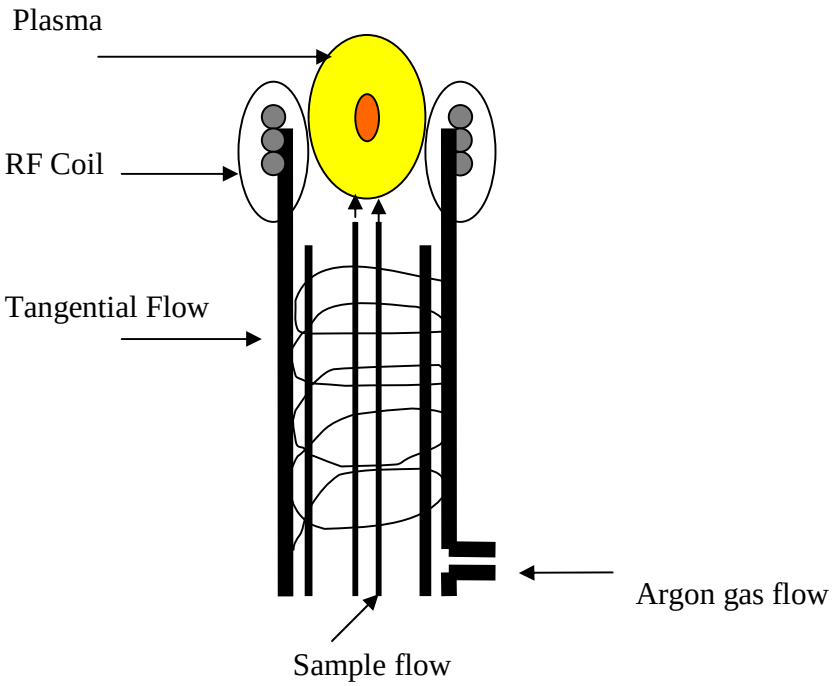

Figure 3. Schematic of ICP Torch

1.1.3 Laser-Produced Plasma AES

Plasmas produced by lasers have similar properties as the ICP plasma, but the formation involves focusing a laser to a point in or on the sample and atomizing and ionizing a small portion (ng to µg) of the sample. A laser pulse creates the plasma which is not continuous but is short-lived. Once formed, it quickly decays by expanding outward at supersonic speeds. The plasma is formed *each* time the laser sparks or pulses and quickly decays in approximately 10 microseconds (µs). The duration of a laser pulse is typically 10 nanoseconds (ns). A laser-produced plasma is often referred to as a *plasma plume* due to its rapid expansion and the continuum of radiation that is produced.[5]

Multi-photon ionization and electron collisions that lead to cascade breakdown are the processes involved in generating a laser-produced plasma. Plasmas are generally

described as being partially ionized gases due to the ions and atoms that are formed from the atomization and ionization of the sample. The temperature of the plasma is highest when it's first formed and at this time there are usually no characteristic atomic emission lines of the element(s). The detector system is typically set to collect data after local thermodynamic equilibrium has been established. After this time, the atomic emission lines of the analyte elements are available. The Detector System is an important component in characterizing plasmas (see section below on Detector System). Gating the detector can avoid the detection of the continuum of radiation emitted by the early plasma. The detector system determines the limit of detection along with other factors such as the plasma atomization/excitation temperature and the power of the laser. Laser-produced plasmas are used widely as atomization and excitation sources in elemental analysis of various samples including heavy metals in soils, liquids, and other solids. One of the major advantages of using this technique is that the high temperature of the plasma provides adequate thermal energy for optical emission.

1.1.3.1 Plasma Decay and Electron Density

The plasma created by the laser pulse/spark has a characteristic that is a function of the electron density and time. Plasmas produced by lasers have relatively high electron densities that decay with time.[6] The electron density and plasma temperature decrease as the plasma decays. The Boltzmann equation can be used along with emission measurements to determine the temperature of a plasma.[7] The electron density of plasmas can be characterized and/or measured using Stark broadening of the H_α-line (pronounced H alpha line).[8] This is a red spectral line produced by hydrogen atoms that

is often used for characterizing different kinds of plasmas. Due to the characteristic of the line often being considered optically thick, many researchers have not used H_α-line to determine electron density in laser-produced plasmas on solids.[8,9] However, other researchers have found that the H_α-line is useful when measured under optically thin conditions. Stark broadening of hydrogen emission lines can be used to evaluate the electron density in the laser-produced plasma.[10] In this work, the instrument parameters have been optimized to show characteristics of the electron density in the laser produced plasma as it decays over time with hydrogen, selenium, and antimony.

1.1.4 Laser Induced Breakdown Spectroscopy, LIBS

LIBS is an AES technique that uses a laser-produced plasma as an atomizer and excitation source. The plasma is formed and atomization and excitation occur as discussed in the section above on laser-produced plasmas. Sample preparation is usually minimal in LIBS. Solids and even liquids and gases can be directly analyzed without sample preparation or minimum if any. Field-portable technology can be used for many applications for measurements in the environment, air, and soil.[11] Real-time and in-situ analyses are possible with the LIBS technique. In these studies, the use of LIBS coupled with a sample introduction technique termed hydride generation has been evaluated. Hydride generation will be discussed in detail below.

1.1.5 Comparison of AES Techniques

Many techniques and methods exist in AES and some have advantages over others. The application determines the method or technique that is required. The

atomization and excitation sources are the thermal energy supplier(s) of all AES techniques. There are essentially three categories for sources of thermal energy in this form of spectroscopy that include flame, furnace, and plasma.[1,2] Flames are useful for group 1A and 2A elements because they're easier to ionize. Flames provide the lowest sensitivity due to their temperatures not being as hot as furnaces and plasmas. Single element analysis is usually the limitation of Flame-AES. Furnace atomizers are more sensitive than flames and provide lower detection limits. The sample size is usually minimal when using furnaces such as graphite furnaces and is an advantage for these atomizers.[4] Multi-elemental analysis is possible with furnaces and interference from the source is minimal. Plasmas are excellent sources for thermal energy due to their high temperatures. The sensitivity of the methods of ICP and LIBS is high when used with sample introduction techniques to separate the sample from its original matrix.[12,13] As discussed above, both LIBS and ICP utilize a plasma as the atomizer and excitation source, but there are advantages of using LIBS over ICP. These advantages include measurement capabilities of solids, liquids, and gases. ICP allows for the measurement of solids and gases, but the effectiveness of the method is best with aqueous samples. LIBS requires little or no sample preparation and only a small size of the sample is required for measurement. ICP usually requires sample preparation and the sample size required is relatively large compared to the ng/µg sample size of LIBS. Last, but not least, the instrument for ICP is generally not portable. However, an instrument for LIBS can be made as a portable device for field use. Table 1 lists some of the different AES techniques and the typical excitation temperatures. Drawbacks or disadvantages of plasmas being used as atomizers and/or the excitation source, as in LIBS, are the

interference caused by atmospheric gases such as oxygen, nitrogen, and hydrogen. LIBS also usually has detection limits in the ppm range unless it is used with other methods to increase the sensitivity.

In AES thermal energy is required for optical emission of elements. The thermal energy source(s) must be capable of efficiently atomizing and exciting atoms for good results to be obtained. The research in this work involves coupling a sample introduction technique known as hydride generation to a laser-produced plasma method as in LIBS.

AES Technique	Temperature (K)
LASER PRODUCED PLASMA	10000
ICP	4000-8000
FLAME	1500-2500
SPARK AND ARC	3000-8000
MICROWAVE INDUCED PLASMA	1000-2000
GRAPHITE FURNACE	2000

TABLE 1. Common AES Techniques

1.2 DETECTOR SYSTEM

AES requires a system that detects the emitted radiation of elements during analysis. The detector system is a determining factor for the limit of detection in elemental analysis. The detector system in these studies consists of a monochromator and a photomultiplier tube, PMT. The monochromator is an optical device that can be

adjusted in order to transmit specific bands of wavelengths of light from a range of wavelengths.[5] A diffraction grating is used to separate bands or colors of light and direct the selected wavelength through an exit slit. The PMT is the detector of light and it is positioned at the exit slit of the monochromator to detect the light; it is very sensitive to UV/VIS and near infrared light. The PMT consists of a photo-sensitive cathode and a series of dynodes. The individual photons of light received from the monochromator hit the photocathode of the PMT and photo-electrons are emitted. The photo-electrons accelerate towards the first dynode and secondary electrons are created each time an electron hits a dynode.

An electronic device, known as the Boxcar Averager, converts the analog signal of the PMT to a digital signal via a computer interface. When displayed, the digital signal is used to determine emission peak(s) of element(s) in the sample. The Boxcar Averager settings are used to optimize parameters such as gate width and time delay. These parameters must be set and optimized correctly in order to determine when the best emission data can be obtained from the light detector system. The detector is constantly receiving light from the monochromator and the time delay and gate width are parameters that correspond to a selection or gate of time of the signal.[9] The time delay, or delay, is a setting corresponding to a time after the laser pulse occurs. As discussed earlier, the plasma is formed with each laser pulse or spark; hence, the delay is related to emissions occurring in the life of the plasma. This setting directs the Boxcar Averager to acquire the signal from the detector during a specified time after the laser fires. The gate width setting corresponds to the length of time the signal is to be collected. The delay and width settings are used to gate the detection of the emission process. Because plasmas

have dynamic properties, it is useful to know when to obtain measurements of the emitted radiation from the excited atoms. Changing and optimizing parameters such as gate width and delay allows an analyst to determine the best time to collect measurements from the plasma.[9] Figure 4 shows a diagram of the detector system used in this work.

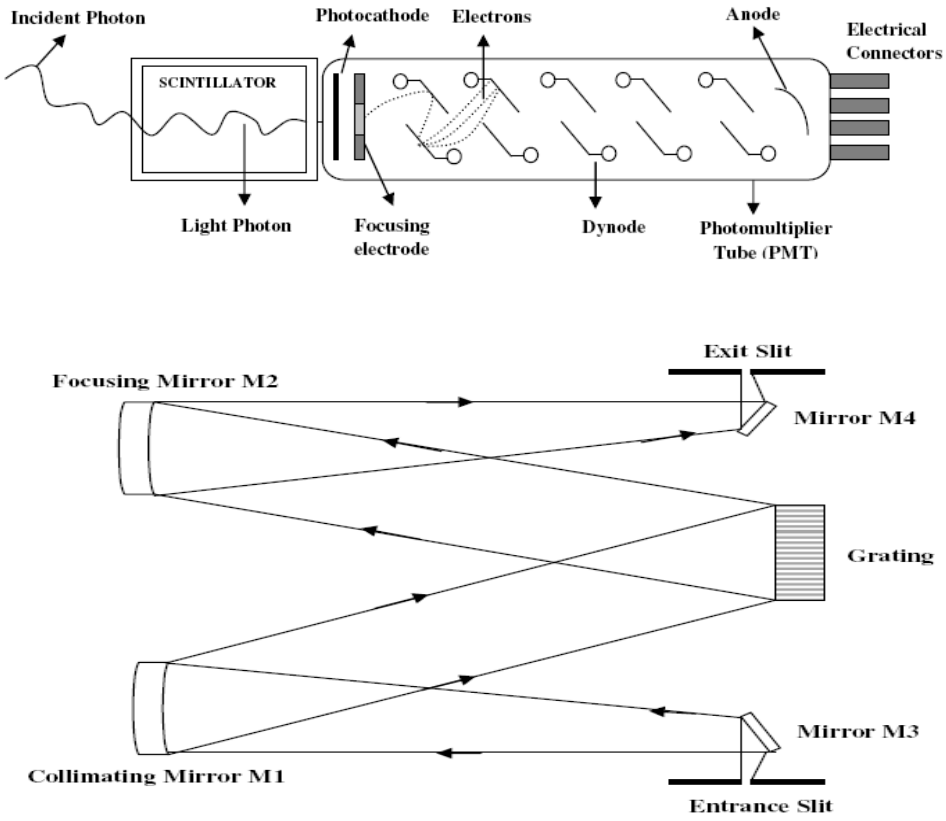

Figure 4. PMT, top; Monochromator, middle; System Diagram, bottom

CHAPTER 2: SELENIUM AND ANTIMONY

2.1 SELENIUM, Se

Selenium is a mineral element that is found in the environment and occurs from natural or anthropogenic sources. The atomic number of Se is 34, its atomic mass is 78.96 and it is chemically related to sulfur and tellurium.[14] Se is a nonmetal and rarely occurs in its elemental (insoluble form) state in nature. Selenate, selenite, and selenade are inorganic forms of Se that occur naturally. The element is found in natural sources mostly in rocks and soils usually combined with sulfide, copper, lead, or other minerals.[15] Environmental matrices contain Se at concentrations ranging from mg/kg down to ng/kg.[15] Anthropogenic sources include smelting of ores and other similar pollution activities. Se has a biological role in human health; low doses are essential to good health and high doses can have adverse effects. Se plays a key role in the metabolism of plants, animals and humans by its incorporation into active enzymes.[15] Se plays a role in biological systems that is analogous to sulfur; it is found in organic compounds such as dimethyl selenide, selenomethionine, selenocysteine, and methylselenocysteine. Exposure typically comes from food consumption, but at very low levels that are not harmful. On the contrary, high levels of exposure or ingestion can result from living near industrialized areas that pollute the air or water. Trace analysis of selenium is essential to help control air and environmental pollution. According to the guidelines of the U.S. EPA, the maximum allowable concentration of Se in drinking water is 10 ug/L.[16] Blood and urine samples can be analyzed for trace amounts of Se to determine the toxicity level in the biological system. Selenosis is a condition resulting from high blood levels of Se (greater than 100 ug/dL).[17] This condition includes symptoms such as gastrointestinal

upsets and hair loss. The toxicity of Se depends on its chemical form. Se is measured in this research using Hydride Generation Coupled with LIBS or HG-LIBS. The Se in solution is separated from the matrix and converted into hydrogen selenide gas.[18,19] In these studies, Se species in solution are converted to H_2Se that is atomized and excited by a laser-produced plasma and the optical emission is measured at a selenium-specific wavelength near 196 nm. Optimization of the instrument to obtain the maximum wavelength of emission was performed using a 10 ppm solution of Se. The optimized parameters were used to measure various concentrations of Se ranging from 0 to 10 ppm to create a calibration curve.

2.2 ANTIMONY, Sb

Antimony, Sb, is a chemical element with atomic number 51 that is classified as a metalloid. Sb is not an essential element for biological systems or plants and it has cumulative toxicity properties.[20] The toxicity of Sb depends strongly on its chemical form or oxidation state; Sb in its elemental form is more toxic than its salts.[20] The four oxidation states include Sb^{-3}, Sb^{0}, Sb^{+3}, and Sb^{+5}; the +3 state is the most common and most stable. Sb has toxic effects and chemical behavior similar to that of arsenic.[21] Due to the different states/forms that Sb can exist, it's important during trace chemical analysis to identify and quantify each chemical form. Illnesses such as pneumonitis, fibrosis, bone marrow damage and carcinomas have all been reported as a direct result of inhalation exposure to Sb in its toxic forms. Sb can be introduced into the environment through human activities such as mining and smelting and also from rock weathering and

soil runoff. Sb is primarily used in ceramics and glass, in flame retardant materials, and in plastics.[22]

In natural waters, the concentration of Sb is typically less than 1 µg/L, which is considered a low level of pollution; antimonate and antimonite are two common inorganic forms found in natural water.[22,23] Sb has been largely overlooked as an environmental concern in pollution of waters and soils due to its compounds being relatively insoluble. The U.S.EPA has a limit of 0.006 mg/L of Sb in drinking water. Biological systems containing Sb (in excess of the minimum concentration level allowed) for several years can sustain damage to the central nervous system.[24] Speciation of Sb can be achieved by various means including HG-ICP-AES, HG-AFS (hydride generation atomic fluorescence spectrometry), and ETV-ICP-AES (electrothermal vaporization inductively coupled plasma atomic emission spectrometry).[20]

CHAPTER 3: GOAL OF THE PROJECT

The long term goal of this research project is to develop a method or methods to speciate and detect low concentrations of elements such as Se and Sb. The elemental analysis involves the analyte in solution being converted to a volatile gas via hydride generation. The hydride generation approach is a sensitive sample introduction technique and may be useful for trace analysis when combined with LIBS. The long term goal of the project is to include separation by HPLC with HG and LIBS or LIF techniques. Metalloids such as Se can be separated or speciated into different seleno-compounds or different forms of Se to include different oxidation states. Separation of Se species can be performed effectively with HPLC methods and sensitive detector systems.[14] The short term goal of the project is to evaluate HG-LIBS for the detection of trace Se and Sb in solution. HG-LIBS research was performed by optimizing instrument parameters such as time delay and time width and studying the plasma characteristics of the laser-produced plasma for the maximum emission intensity peak of Se and Sb. Ethanol was investigated as an additive to possibly enhance the emission of the Se atoms in solution.[25]

CHAPTER 4: EXPERIMENTAL

4.1 HYDRIDE GENERATION-LASER INDUCED BREAKDOWN SPECTROSCOPY, HG-LIBS

Hydride generation, HG, is a useful sample introduction technique for atomic spectrometry analysis because this technique can significantly increase the sensitivity. The hydride approach can also be helpful in chemical speciation for metalloids during elemental analysis.[12] The sensitivity is increased due to the high sample conversion efficiency from analyte in solution to a gaseous hydride that is carried to the atomizer for analysis. The conventional methods of AES deliver the analyte to the atomizer via a process called nebulization. In this process, the analyte in solution is converted into an aerosol and small particles or droplets of the analyte are formed. This conversion allows for a only small percentage of the analyte to be converted and the remainder of the solution flows to a waste receptacle. Hydride generation converts nearly 100% of the analyte into its hydride form via a chemical reaction. In this work, aqueous solutions of Se and Sb are converted into a volatile hydride of the metalloid by mixing with sodium borohydride ($NaBH_4$) and hydrochloric acid (HCl) via a reduction reaction. For Se, volatile hydrogen selenide (H_2Se) is formed and flows continuously into the optical cell for measurement. The hydride is carried via an inert gas, namely Argon. A hydride generator apparatus including a peristaltic pump (figure 5) is used to make the hydride of the analyte. The *general* hydride generation reduction reaction is as follows:

$NaBH_4 + 3H_2O + HCl \rightarrow$

$H_3BO_3 + NaCl + 8H + E^{m+} \rightarrow H_nE + H_2$ (excess); **E** is the analyte, **m** may or may not be equal to **n**

The AES technique known as Laser Induced Breakdown Spectroscopy, LIBS, is used to quantify or determine the analyte. The laser produces powerful laser pulses that form the plasma in or on the hydride. The laser pulse, or spark, is non-continuous and is formed at the laser repetition rate of 10Hz. The LIBS technique has the ability to measure samples such as liquids and solids without prior preparation. The plasma temperature is approximately 10,000 K during the laser ablation process. The atomic emission of the analyte is achieved by atomization and excitation from the plasma.

4.1.1 Peristaltic Pump

A peristaltic pump uses positive displacement to pump a variety of fluids. In this work, a four channel peristaltic pump (Dynamax, Rainin Instrument Co. Inc.) was used to pump the solutions at a constant rate to the mixing chamber for the reduction reaction. All solutions were in separate beakers with tubing set into each for aspiration. The sample was delivered to the hydride generator at a rate of 8mL/min. The peristaltic pump was used to control the flow rate based on different diameters of tubing. The complete HG apparatus consists of the peristaltic pump, the gas liquid separator and a nafion tube dryer.

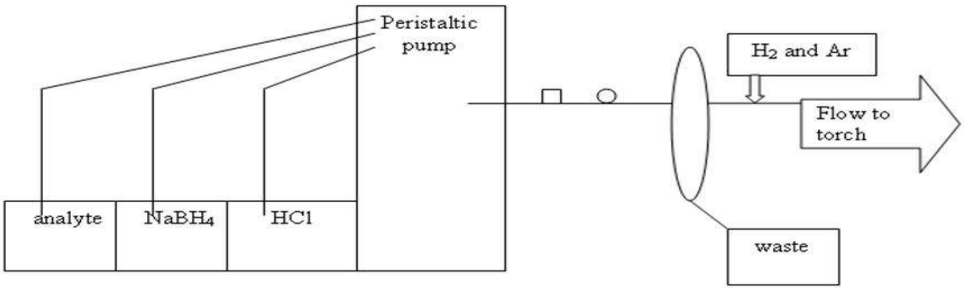

Figure 5. Hydride Generator Apparatus

4.2 LASER SYSTEM

An Nd: YAG laser (Surelite SL-II10, Continuum or Spectra Physics DCR 2A) is used in this research. The laser operates at 10Hz or 10 pulses per second. The typical wavelength to emit light using this type of laser is 1064 nm which is near infrared light. The second harmonic (used in this work) of 532 nm is generated from the frequency doubling of the high-intensity pulses. See figure 6 for the schematic of the laser system.

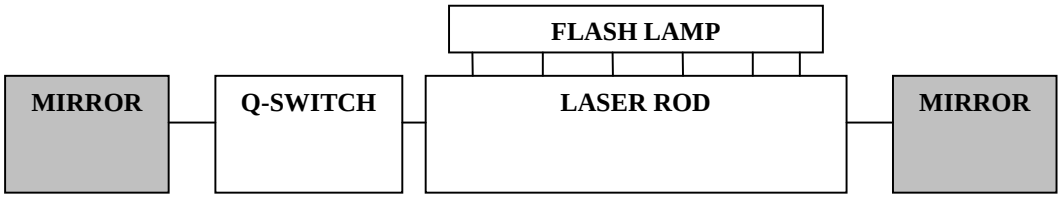

Figure 6. Schematic of an Nd: Yag LASER Configuration

CHAPTER 5: MATERIALS AND METHODS

5.1 REAGENTS AND STANDARDS

Selenium calibration solutions were prepared from standard reference stock solutions of Se (1000 ppm ± 1%, Fisher Scientific). Calibration solutions prepared from the stock solutions were further diluted by serial dilution to make reduced concentrations. De-ionized water obtained from the laboratory's de-ionized water supply was used as the water for making **all** solutions. Antimony calibration solutions were prepared from standard reference stock solutions of Sb (1000 ppm ± 1%, Sigma Aldrich).

The sodium borohydride solution, $NaBH_4$, was prepared using $NaBH_4$ pellets (AF granules, 10-40 mesh, 98%, Sigma Aldrich). A 250mL, 1.5% borohydride solution was prepared by dissolving 3.75g of $NaBH_4$ in 250 mL of de-ionized water; the solution was stabilized by the addition of 0.4% (m/v) NaOH pellets (Fluka). The 10% HCl solution (250 mL) was prepared by adding 67.5 mL of concentrated HCl (35%-38% v/v, Pharmaco Aaper) to a 250 mL volumetric flask (half filled with de-ionized water) and diluting to volume with de-ionized water; the solution was mixed well.

Ethanol solutions were prepared from ethyl alcohol, 200 proof, anhydrous, 99.5 %+. Ethanol solutions were added to 10 ppm solutions of Se and the responses were plotted against the % of alcohol added.

5.2 PROCEDURE: HG-LIBS

5.2.1 Emission Peak

Instrument parameters were adjusted for optimization of the method to analyze selenium, antimony, and hydrogen. Two different laser energies were used during element analysis at the second harmonic of 532 nm. The "lower energy" corresponds to approximately 30 mJ and the "higher energy" corresponds to approximately 140 mJ. In this work, the lower laser energy is used unless otherwise specified as the higher laser energy. The set parameters were established to obtain the maximum emission peak at an element-specific wavelength or wavelength range along with a scan rate (nm/minute). The following boxcar parameters were adjusted for optimization of the method: time delay (t_d), time width (t_w), signal, and averaging. The slit width and wavelength were adjusted on the monochromator.

A 10 ppm aqueous solution of analyte (Se, Sb) was prepared in a 1 liter volumetric flask and approximately 250 mL of the sample was transferred to a beaker to be used for the analysis. A 250 mL beaker of deionized water was used for hydrogen analysis. Three separate beakers with volumes of 250 mL each of sample solution, sodium borohydride solution (1.5%), and HCl solution (10%) were connected to the peristaltic pump via aspiration tubing. The pump was set to aspirate the solutions and generate flow to a mixing block for the reduction reaction to occur. In the case of Se, H_2Se gas was formed in the reduction reaction and carried to the torch by argon, an inert gas. The remaining solution flowed to a waste receptacle.

The plasma was formed by the laser at the torch in the flowing gas mixture. The heat of the plasma atomized the gas forming free atoms which were also excited from the heat of the plasma. The analyte atoms gained enough energy and were promoted to an excited state from the ground state. As the excited atoms returned to a lower energy or

ground state, light was emitted by the atoms and detected by the detector system. The detector system, in conjunction with the boxcar averager, detected and converted the light to an analog signal. This analog signal was converted to a digital signal via a computer interface and an emission spectrum was graphed from the data.

5.2.2 Generation of a Calibration Curve

A calibration curve of each analyte solution (not including hydrogen) was generated from solutions of the analyte ranging from 1 ppm to 10 ppm with 0 ppm as the *blank*. Each solution was analyzed following the above steps in section 5.2.1 for the maximum emission peak. The *blank* solution was analyzed to obtain baseline results of the technique and to account for interferences. The calibration curve was used to determine the limit of detection, LOD. The graph of the calibration curve shows a plot of emission intensity versus concentration.

CHAPTER 6: RESULTS AND DISCUSSION

6.1 HYDROGEN EMISSION SPECTRA

In order to evaluate the plasma characteristics, including the electron density, hydrogen emission spectra were obtained from the hydride generation sampling technique coupled to LIBS. The procedure for this technique was discussed in detail in the section, *Emission Peak.* Instrument parameters were adjusted to give maximum emission intensity of hydrogen at a wavelength of 656 nm at both lower and higher laser energies. Table 2 provides the conditions employed during the generation of hydrogen emission peaks at the lower laser energy. The monochromator was adjusted to a wavelength range of 650-660 nm at a scan rate of 5 nm/minute. Figure 7 shows the hydrogen emission peak at 656 nm with the maximum emission intensity under the conditions employed in table 2. Table 3 provides information on the instrument parameters and conditions that remain constant throughout the measurement process for ***all*** elements at both laser energies.

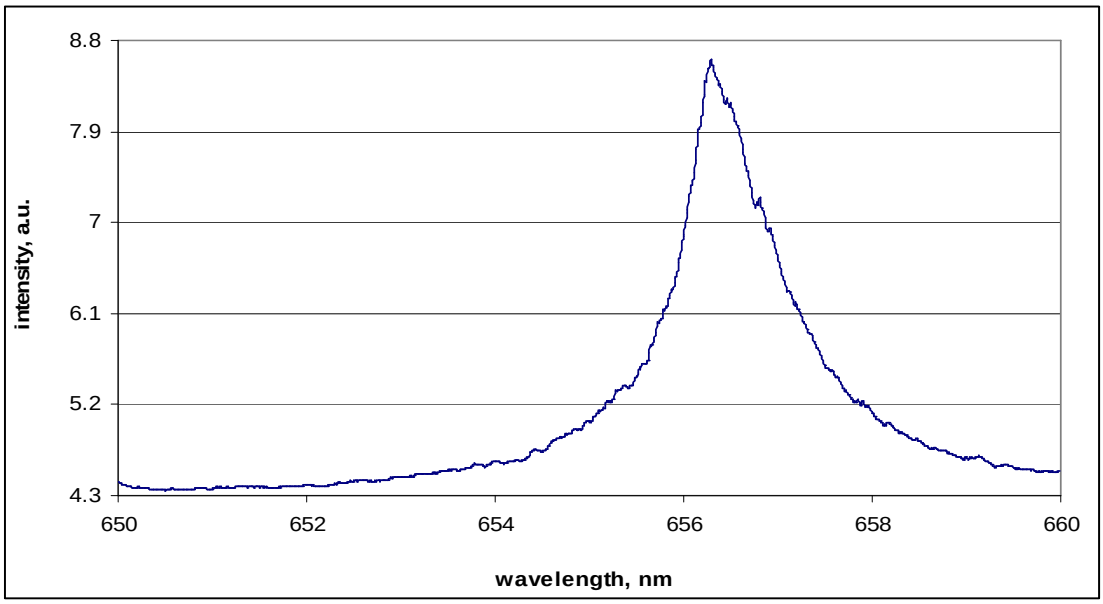

Figure 7. Hydrogen emission peak – 1

500 ns delay, slit width 20 µm, averaging 30, signal 10 mV/V

t_d, µs/ns	t_w, µs	Averaging (Avg)	N.D. filter	Slit width, µm	Signal, mV/V	Max. intensity, a.u.
500 ns	3	30	1.3	20	10	3.88
700 ns	3	30	1.3	20	10	3.62
1µs	3	30	1.3	20	10	2.88
3µs	3	30	1.3	20	10	0.85

TABLE 2. Instrument Parameters for Hydrogen Emission Peaks

%$NaBH_4$	%HCl	PMT, V	Flow Rates of Ar, sccm
1.5	10	-1200	40,40

Table 3. Constant Instrument Parameters and Conditions

Additional hydrogen emission spectra were collected using varying conditions to include neutral density (ND) filters, different monochromator slit widths and time delays. Table 4 provides instrument parameters for figures 8-12 for the lower laser energy. Inspection of these spectra shows that the time delay parameter affects the apparent peak intensity and broadening.

figure	t_d, µs/ns	Avg	Slit width, µm	Signal, mV/V	ND filter	Intensity, a.u.
8	500 ns	10	20	50	0	5.77
9	500 ns	10	30	20	1.3	5.16
10	300 ns	10	30	50	0.4	6.19
11	100 ns	10	30	50	0.4	6.55
12	700 ns	10	30	50	0.4	6.79

TABLE 4. Instrument Parameters for Figures 8-12

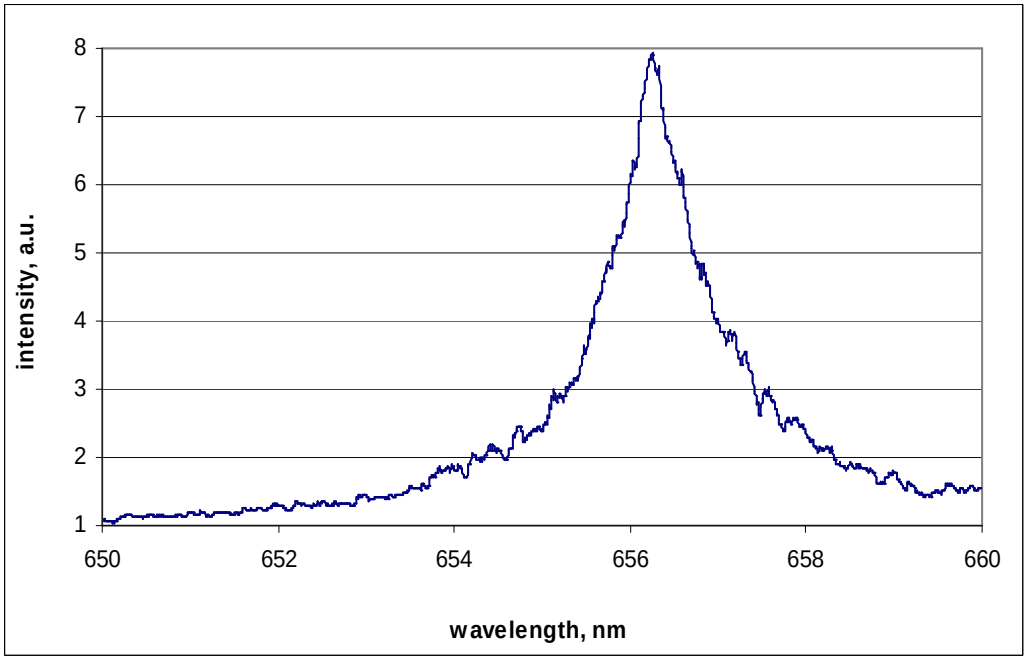

Figure 8. Hydrogen Emission Peak – 2

500 ns delay, slit width 20 µm, signal 50 mV/V

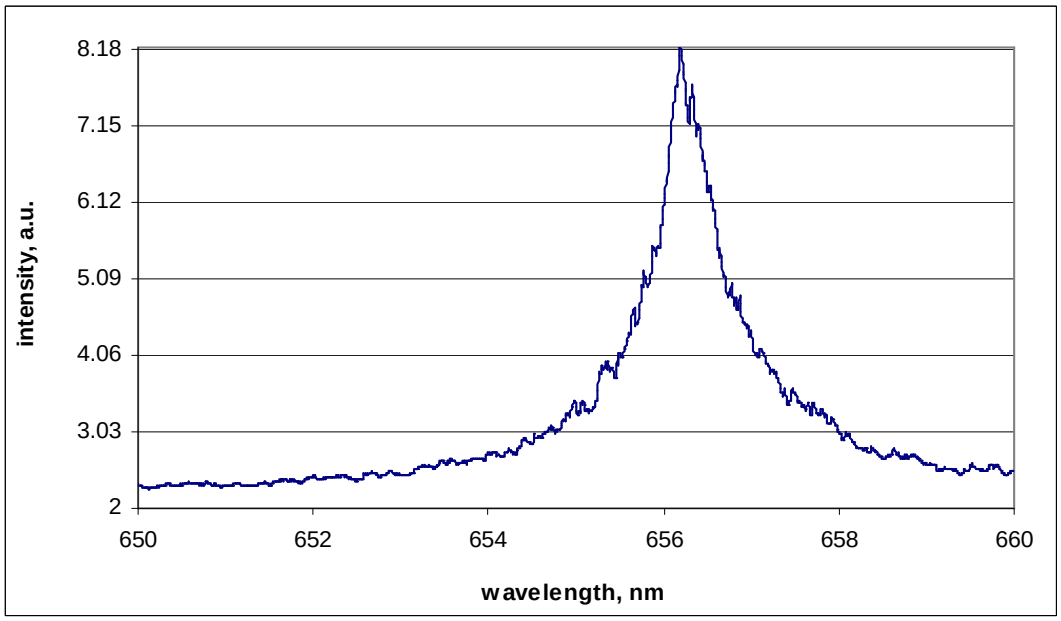

Figure 9. Hydrogen Emission Peak – 3

500 ns delay, slit width 30 µm, signal 20 mV/V, 1.3 N.D. filter

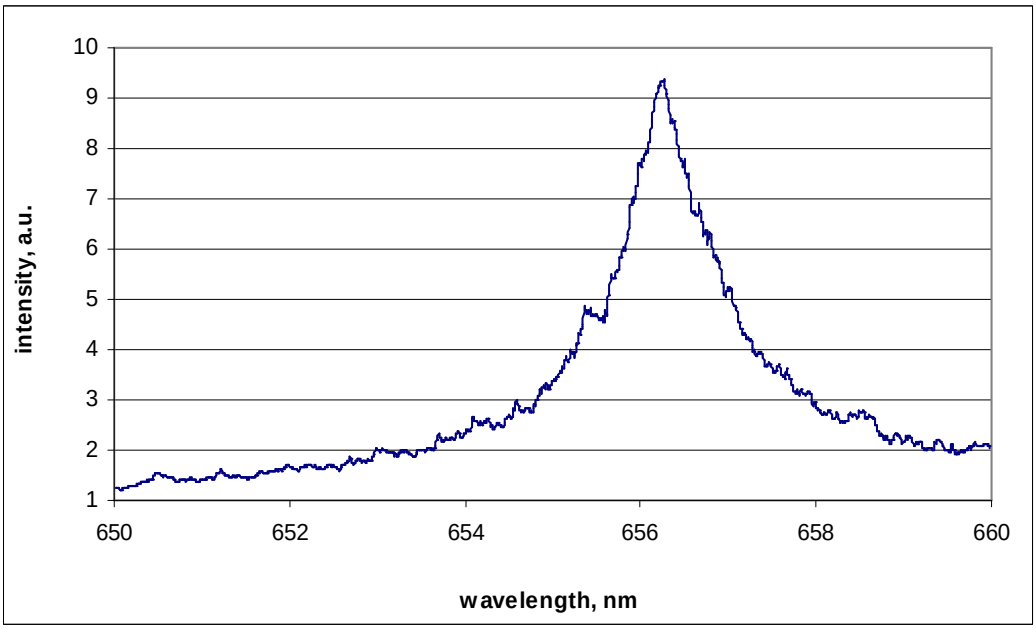

Figure 10. Hydrogen Emission Peak - 4

300 ns delay, slit width 30 µm, signal 50 mV/V, 0.4 N.D. filter

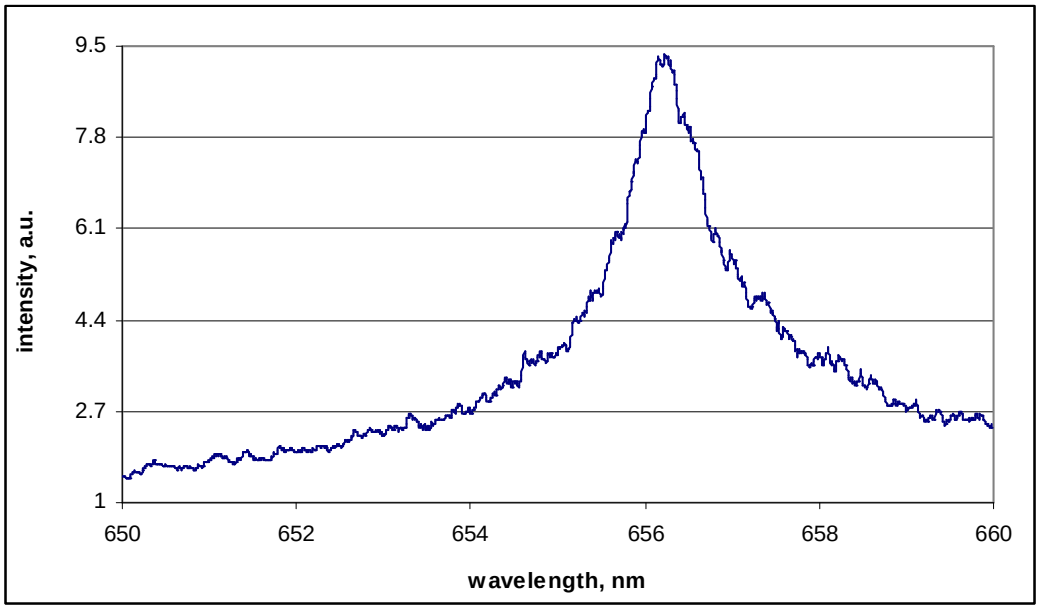

Figure 11. Hydrogen Emission Peak – 5

100 ns delay, slit width 30 µm, signal 50 mV/V, 0.4 N.D. filter

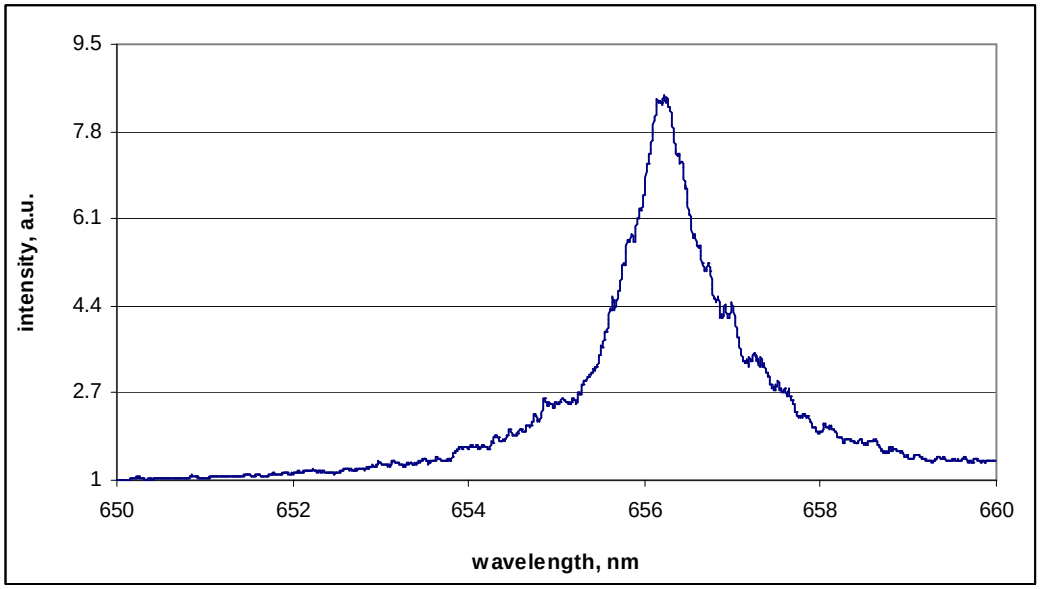

Figure 12. Hydrogen Emission Peak - 6

700 ns delay, slit width 30 µm, signal 50 mV/V, 0.4 N.D. filter

6.1.1 Stark Broadening and Electron Density of Hydrogen Emission Peaks

Adjusting instrument parameters such as the time delay and gate width of the Boxcar Averager produced emission spectra of hydrogen that provided information on the electron density of the plasma. Figures 13 and 14 show emission peaks of hydrogen at the same gate width of 100 ns with different time delays ranging from 100 ns to 5 us and a 2.3 ND filter. The lower laser energy is used and the scan rate was changed to 7 nm/min due to the wavelength range change to 650-665 nm.

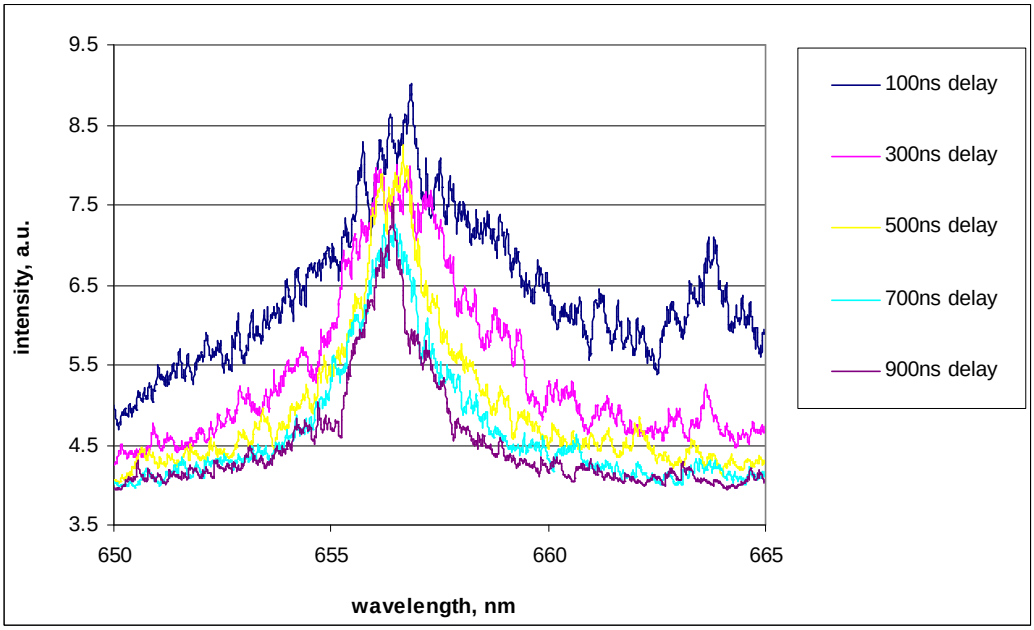

Figure 13. Hydrogen Emission Peaks: Different Time Delays-1

Gate width 100 ns, 2.3 N.D. filter

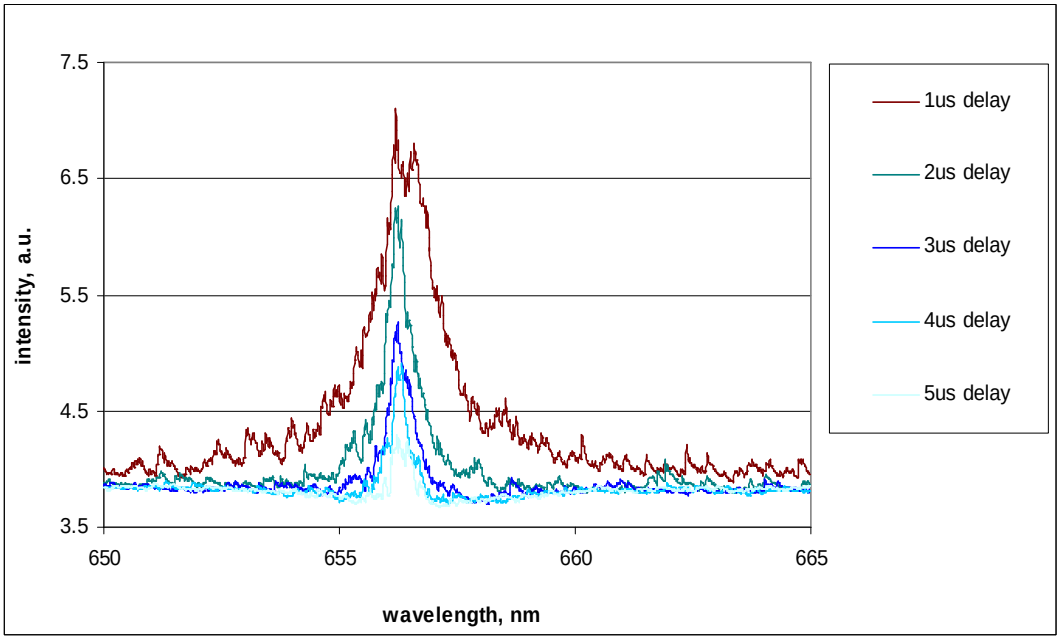

Figure 14. Hydrogen Emission Peaks: Different Time Delays-2

Gate width 100 ns, 2.3 N.D. filter

Figures 15-16 show emission peaks of hydrogen under the same conditions as figures 13 and 14 using the higher laser energy and a 2.4 ND filter. Figure 17 shows the changes in the emission peaks of hydrogen as the time delay increases. A 2.3 ND filter was used during the measurement to attenuate the light. Inspection of the spectra in figures 13-16 shows that the plasma changes over time which causes the emission peaks to change by becoming less intense and less broad.

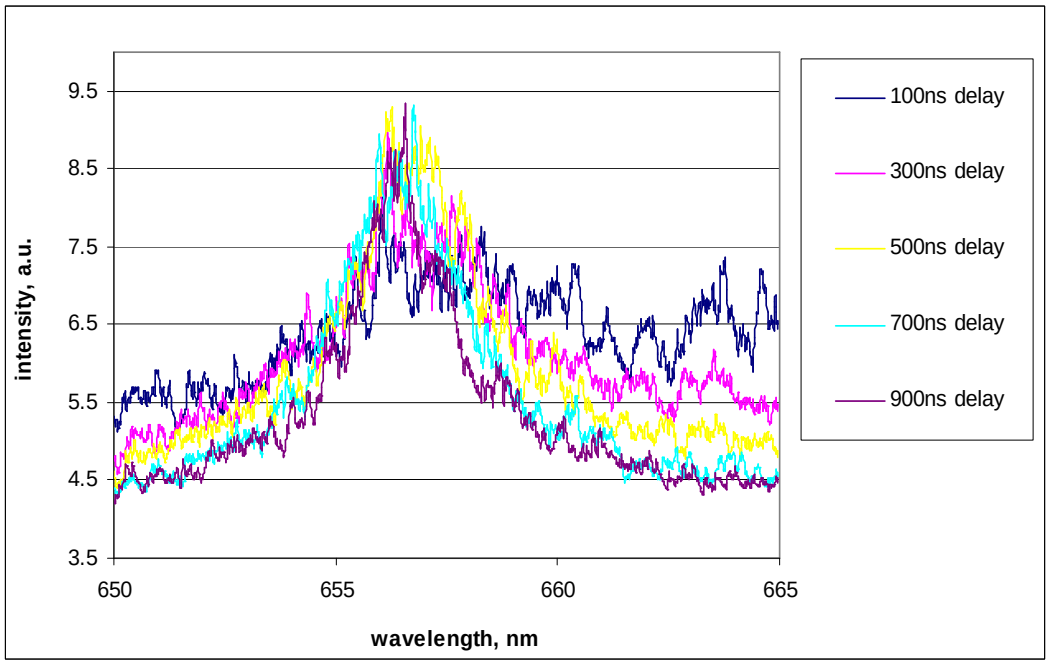

Figure 15. Hydrogen Emission Peaks: Different Time Delays-3

Higher laser energy, gate width 100 ns, 2.4 N.D. filter

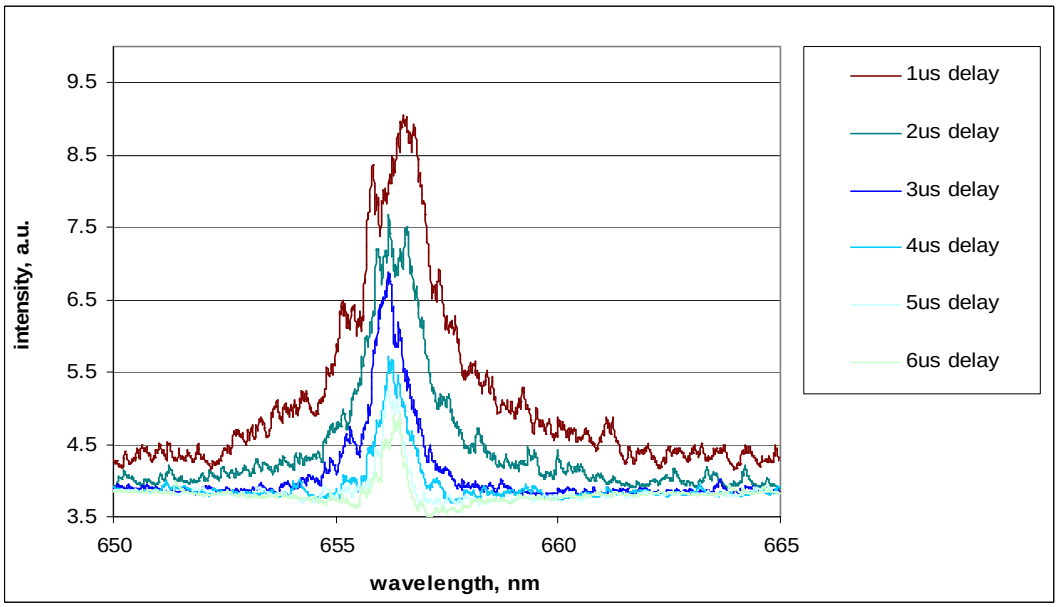

Figure 16. Hydrogen Emission Peaks: Different Time Delays-4

Higher laser energy, gate width 100 ns, 2.4 N.D. filter

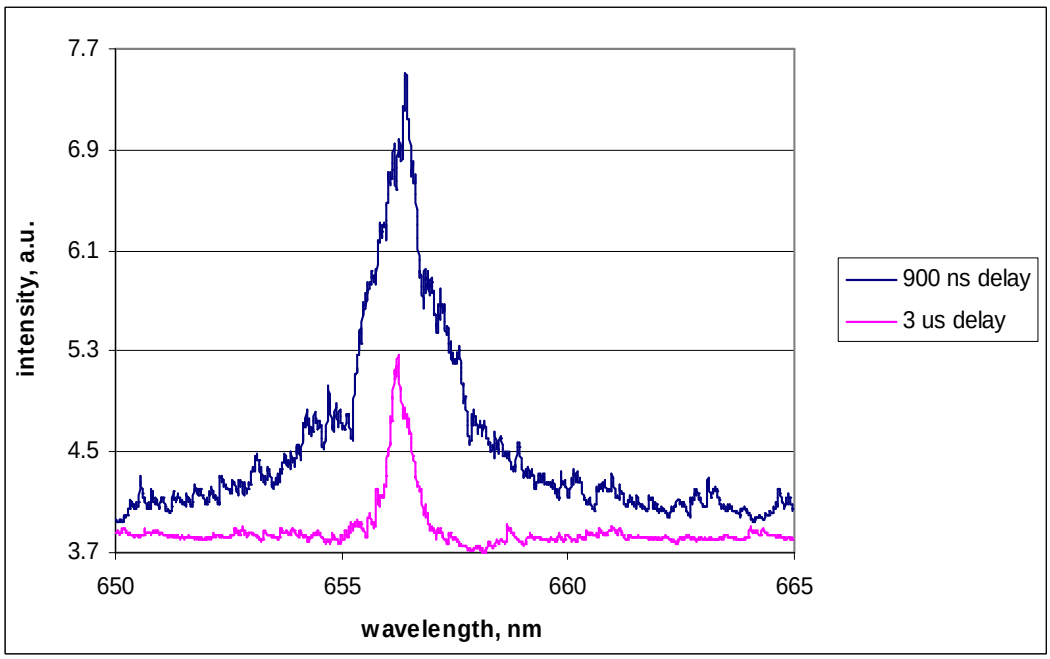

Figure 17. Hydrogen Emission Peaks: Different Time Delays with ND Filter

2.3 N.D. filter,100 ns gate width, averaging 10

6.1.1.1 Plasma Diagnostics

Broadening of emission peaks in plasmas is related to electron density.[26] Electron density calculations begin with processing spectral data and tabulating the full width half maximum (FWHM) value of emission peaks. The full width half maximum value is the width of the peak at half the maximum peak height. Tables 5 and 6 below show the FWHM data and plasma decay time for hydrogen emission peaks of figures 13-14 and figures 15-16 (lower and higher energy respectively). Figure 18 is a plot of the FWHM peak width versus the plasma decay time for values in tables 5 and 6. Tables 7 and 8 show the plasma decay time in ns and electron density in cm^{-3} for the plots in figure 19 for higher and lower laser energy. As described in reference #26, the electron density, N_e, is calculated from the following equation:

$$\mathbf{N_e\ (H_\alpha) = 8.02 \times 10^{12}\ (\Delta\lambda_{1/2}/\alpha_{1/2})^{3/2} cm^{-3}}$$

$\mathbf{\Delta\lambda_{1/2}}$ **= FWHM, angstroms (Å)**

$\mathbf{\alpha_{1/2}}$ **= 0.02**

half maximum height	FWHM peak width, nm	FWHM peak width, Å	Blank corrected FWHM peak width, Å	time delay	ns
7.14	3.42	34.20	34.19	100 ns	100
6.24	2.84	28.40	28.38	300 ns	300
6.20	2.33	23.30	23.28	500 ns	500
5.63	1.81	18.10	18.07	700 ns	700
5.74	1.26	12.60	12.56	900 ns	900
5.55	1.30	13.00	12.96	1 us	1000
4.97	0.57	5.70	5.61	2 us	2000
4.53	0.47	4.70	4.59	3 us	3000

Table 5. FWHM Data for Lower Energy Hydrogen Emission Peaks

half maximum height	FWHM peak width, nm	FWHM peak width, Å	Blank corrected FWHM peak width, Å	time delay	ns
6.85	4.56	45.60	45.59	500 ns	100
7.05	3.28	32.80	32.78	700 ns	300
6.99	3.03	30.30	30.28	500 ns	500
6.82	2.73	27.30	27.28	700 ns	700
6.76	2.12	21.20	21.18	900 ns	900
6.65	1.61	16.10	16.07	1000 ns	1000
5.50	1.45	14.50	14.47	2000 ns	2000
5.40	0.70	7.00	6.93	3000 ns	3000
4.80	0.65	6.50	6.42	4000 ns	4000

Table 6. FWHM Data for Higher Energy Hydrogen Emission Peaks

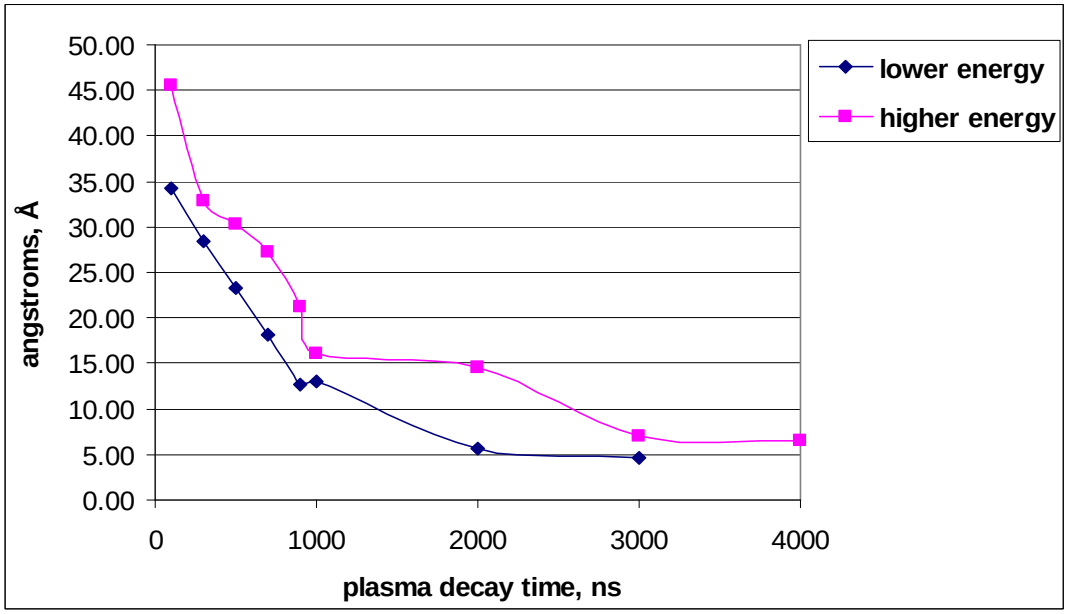

Figure 18. FWHM Peak Width Versus Plasma Decay Time for Lower and Higher Energy of Hydrogen Emission Peaks

ns	N_e
100	5.6686E+17
300	4.2869E+17
500	3.185E+17
700	2.178E+17
900	1.2622E+17
1000	1.3229E+17
2000	3.7677E+16
3000	2.7884E+16

Table 7. Time Delay (ns) and Electron Density (N_e) for Lower Laser Energy

ns	N_e
100	8.72838E+17
300	5.32161E+17
500	4.72458E+17
700	4.04014E+17
900	2.76387E+17
1000	1.82664E+17
2000	1.56075E+17
3000	5.17284E+16
4000	4.69893E+16

Table 8. Time Delay (ns) and Electron Density (N_e) for Higher Laser Energy

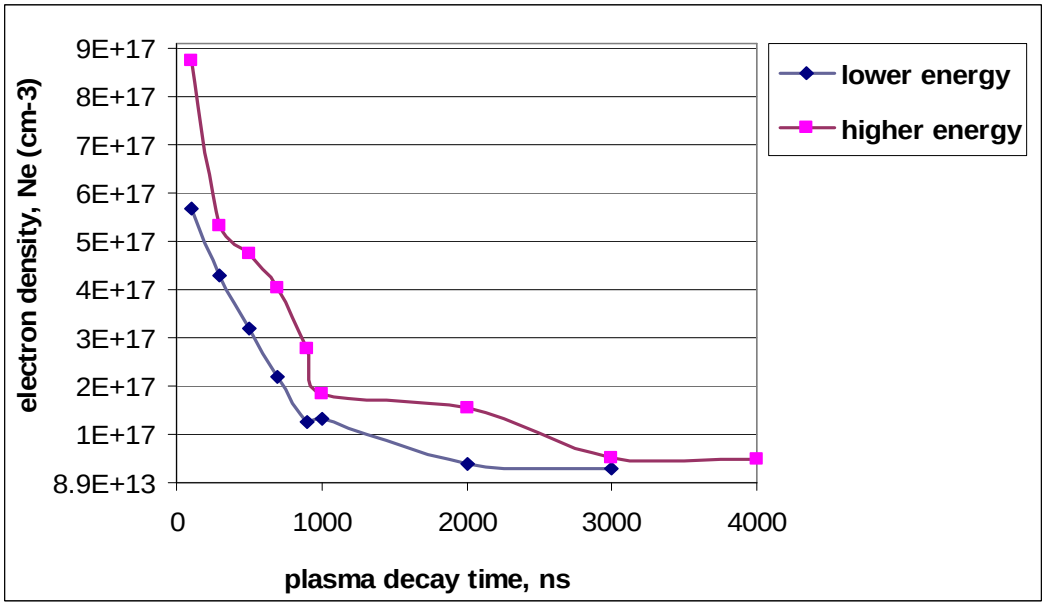

Figure 19. Electron Density Versus Plasma Decay Time for Lower and Higher Energy of Hydrogen Emission Peaks

6.1.2 Discussion

Emission spectra of hydrogen show that the peak width decreases as the time delay increases. The broadening of hydrogen emission spectra is directly proportional to the magnitude of the electric field.[27] The peak width is a function of the electron density which is an important plasma parameter. The temperature of the plasma is highest when it's first formed and cools over time as it decays.

Doppler broadening and Stark broadening are two of the mechanisms that affect line broadening in plasmas.[26] Doppler broadening is a result of the thermal motion of emitting atoms or ions. Doppler widths result from the different velocities of these emitting particles and line broadening results.[26] Doppler broadening depends on the frequency of the spectral line and the temperature and mass of the emitting particles. Doppler broadening is characterized by a Gaussian line shape from a Maxwellian velocity distribution.[10] Stark broadening is a form of pressure broadening and is due to collisions of charged particles.[10] A strong electric field results from the collisions of charged particles and broadening of spectral lines occurs. Stark widths depend on electron density and the relationship is linear. These plasmas are dominated by Stark broadening due to interactions of the atoms with the electric field.

The decrease in the peak width in relation to the increase in time delay is due to the fact that the Stark broadening is seen clearly early in the decay of the plasma when the electron density is high. Figures 13 and 14 show emission spectra of hydrogen at a gate width of 100 ns with time delays ranging from 100 ns to 5 μs. As the time delay increases, the peaks become less broad and the intensity decreases. As time increases, the plasma cools and decays which directly affects the electron density. The electron

density decreases as the time delay increases and this is represented in the peak widths of figures 13-17. Figures 8, 9,10, 11, and 12 have emission spectra from instrument parameters outlined in table 4 to include a signal greater than 10 mV as in table 3. The peak intensity for figures 8-12 are higher than the peak intensities in table 3 due to a higher signal in mV/V.

N.D. filters were used during the measurement process to attenuate the light equivalently and to keep the emission peaks within range of the set parameters of the detector system. Table 4 shows that different filters are needed for different conditions to allow the detector system to collect emissions of light that can be transmitted into usable data. Figures 13-14 and figures 15-16 show emission peaks of hydrogen at lower and higher energies respectively; the peak intensities of figures 15-16 are slightly higher than those of figures 13-14 due to the change in laser energy. The N.D. filters differ by 0.1 for the two laser energies; equal values would cause the peaks for higher laser energy to be out of range.

The FWHM peak width versus plasma decay time calculations were performed on hydrogen emission peaks generated at lower and higher energy for a comparison analysis. The results in figure 18 show that the peak width (in angstroms) decreases as the plasma decay time increases. This data coincides with the earlier discussion of electron density, peak width, and plasma decay. Figure 19 shows that the electron density decreases as the time increases and also that the electron density value for higher laser energy is greater than that for lower laser energy. This difference in electron density is evident at the same time delays for both energies. The FWHM data was not calculated beyond a time delay

of 3 μs and 4 μs for lower and higher laser energy respectively due to adjustments needed on the scan rate of the monochromator.

Table 9 shows results of electron density from this work compared to other work. The data in table 9 shows that the calculated electron densities in this work are comparable to other work using different plasma gases such as methane and hydrogen. The laser energies vary in the table and should be considered in comparisons of the results.

time delay (ns)	H_α width, Å	N_e (10^{17} cm^{-3})	plasma gas	laser energy, mJ	reference
700	19 ± 2	2.0 ± 0.4	methane	75	Parigger, C.G. etal[28]
1000	14 ± 2	1.2 ± 0.3	methane	75	Parigger, C.G. etal[28]
150	38.4 ± 4	5.81	hydrogen	150	Parigger, C.G. etal[29]
250	24.6 ± 2.5	3.25	hydrogen	150	Parigger, C.G. etal[29]
700	not available	2.5 ± 0.4	methane	75	Parrigger and Oks[30]
100	45.6	8.73	argon	~ 140	this work
700	27.3	4.04	argon	~ 140	this work
1000	16.1	1.83	argon	~ 140	this work

TABLE 9. Calculated Electron Densities

6.2 ANTIMONY EMISSION SPECTRA

Emission spectra of a 10 ppm solution of Sb were measured at two different wavelengths to include 252.9 nm and 259.9 nm. The scan rate was set at 1 nm/min and the monochromator was set at a wavelength range of 252-254 nm for the 252.9 nm measurements and the same range was set accordingly for 259.9 nm measurements. Figures 20 and 21 show emission peaks of Sb at the two different wavelengths. The

maximum peak intensity to include minimal background emission was achieved by optimizing the instrument parameters in the same manner as during Se analysis (see below). Table 10 provides instrument parameters for figures 20 and 21.

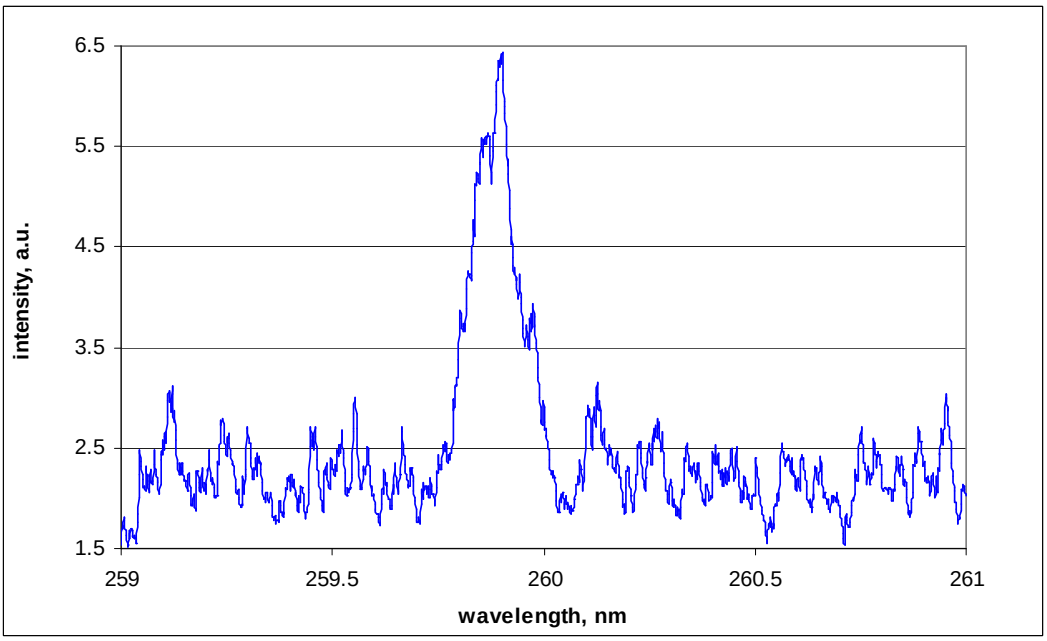

Figure 20. Sb Emission Peak @ 259.9 nm

Time delay 2 µs, gate width 3 µs, slit width 40 µm

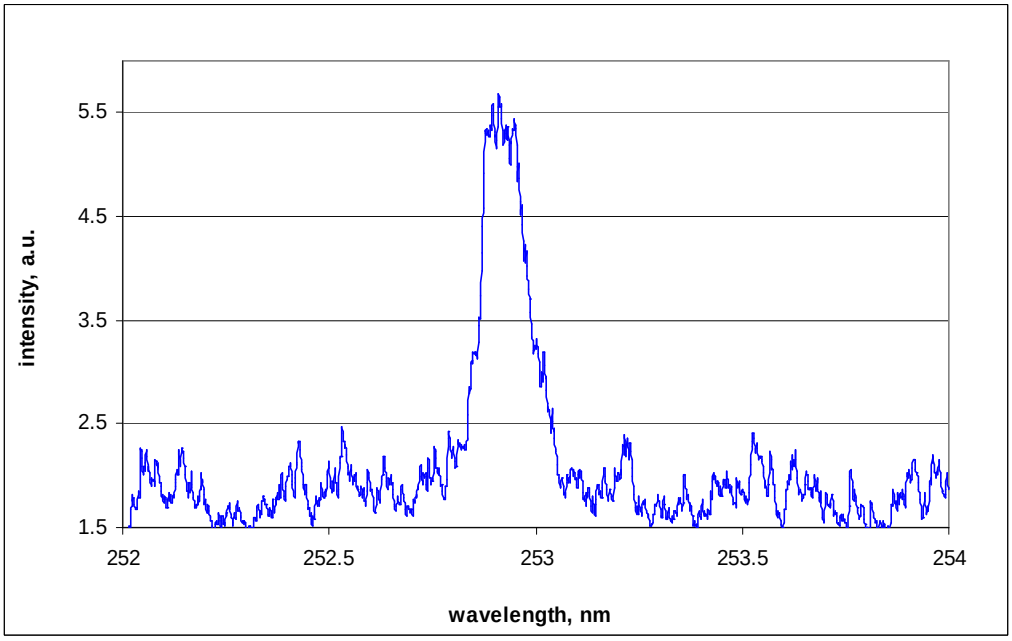

Figure 21. Sb Emission Peak @ 252.9 nm

Time delay 2 μs, gate width 3 μs, slit width 40 μm

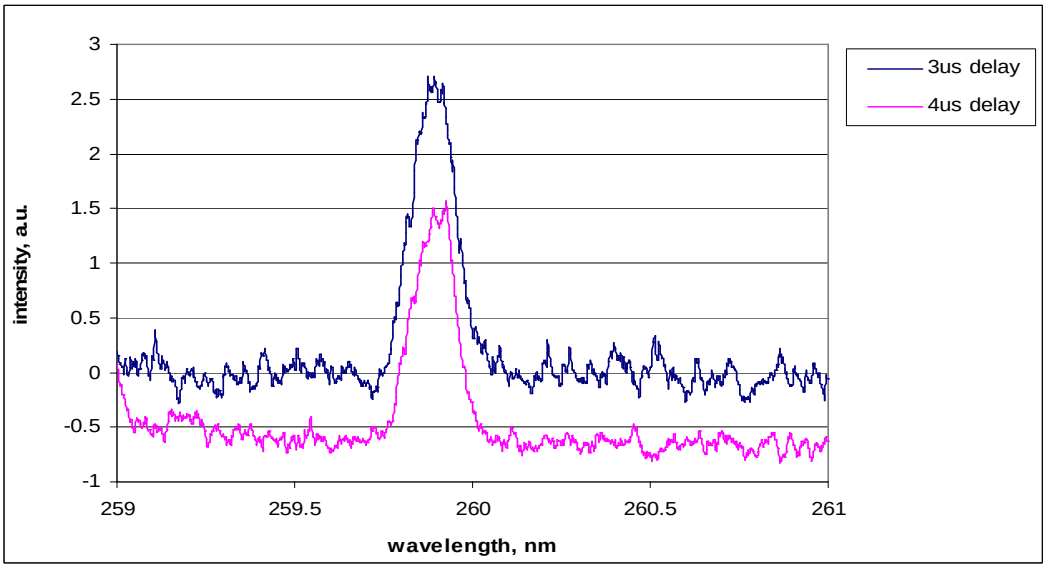

Figure 22. Sb Emission Peak @ 259.9 nm, Different Time Delays

Gate width 3 μs, slit width 40 μm

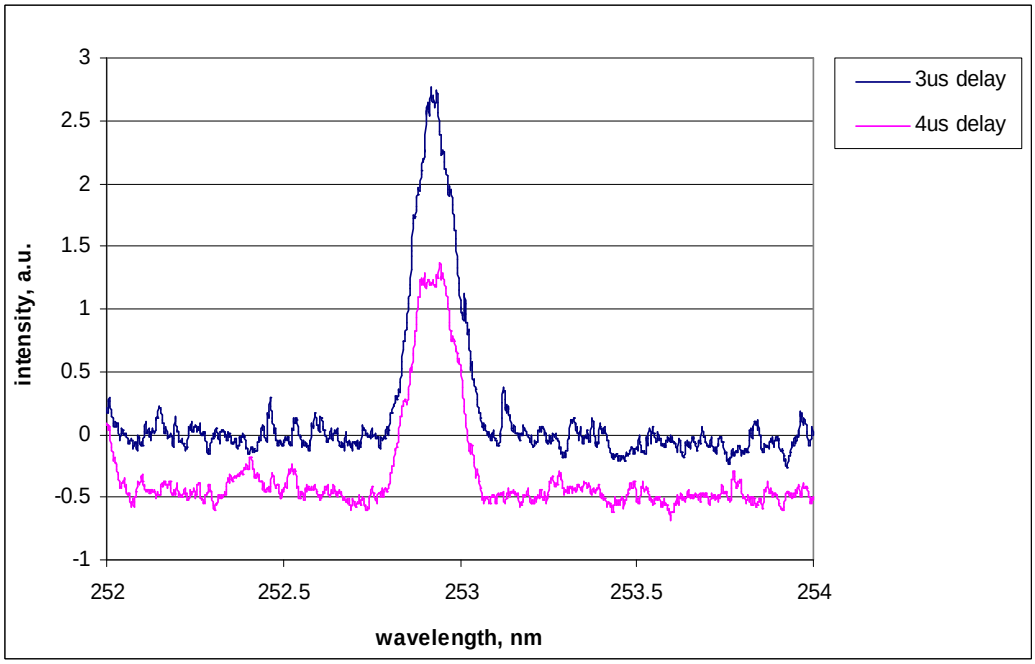

Figure 23. Sb Emission Peak @ 252.9 nm, Different Time Delays

Gate width 3 µs, slit width 40 µm

Figures 22 and 23 are emission peaks for both wavelengths at different time delays. The conditions, other than time delays, for the measurements in figures 22 and 23 are equivalent to those outlined in table 10 for the respective wavelength.

λ, nm	t_d, µs	t_w, µs	Averaging (Avg)	Slit width, µm	Signal, mV/V	Intensity, a.u.
252.9	2	3	10	40	10	3.86
259.9	2	3	10	40	10	4.66

Table 10. Instrument Parameters for Sb at 252.9 and 259.9 nm

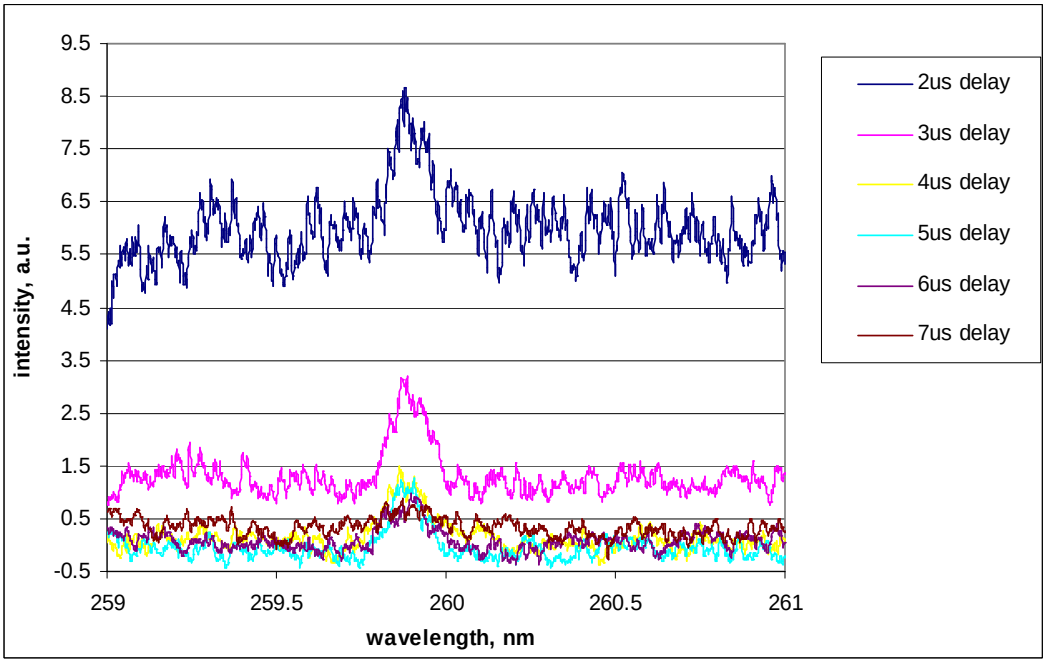

Figure 24. Sb Emission Peaks @ 259.9 nm, Different Time Delays, 100 ns gate width

Slit width 40 µm, 0.4 N.D. filter, lower laser energy

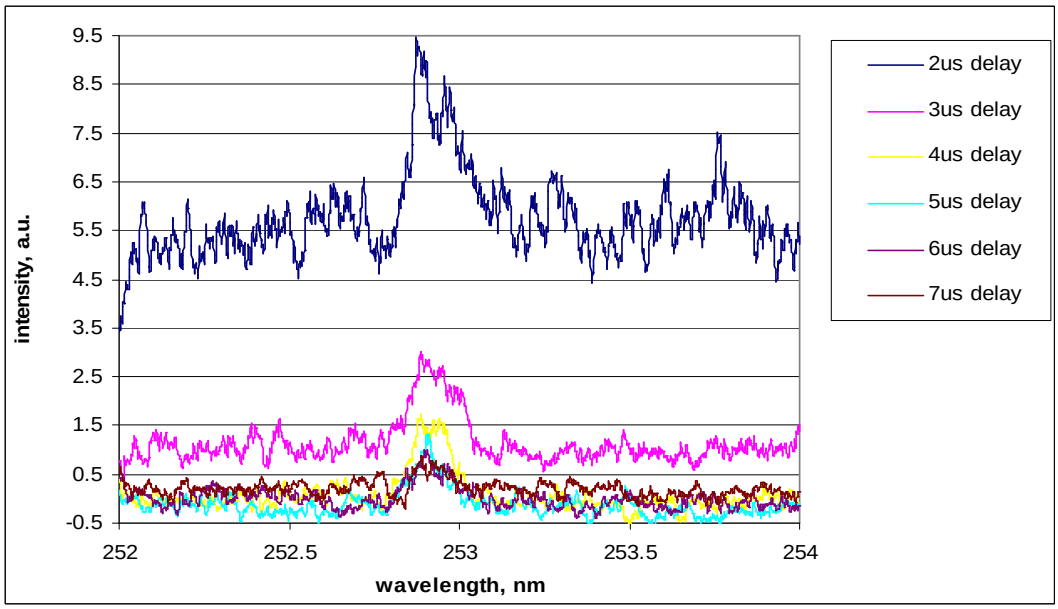

Figure 25. Sb Emission Peaks @ 252.9 nm, Different Time Delays, 100 ns gate width

Slit width 40 µm, 0.3 N.D. filter, lower laser energy

Figures 24 and 25 show emission peaks of Sb at different time delays with a gate width of 100 ns at the lower laser energy. The conditions, other than time delay, gate width and N.D. filters, were equivalent to those in table 10 for the respective wavelengths. A 0.4 N.D. filter was used during measurements for 259.9 nm and a 0.3 filter was used during 252.9 nm measurements in the two figures.

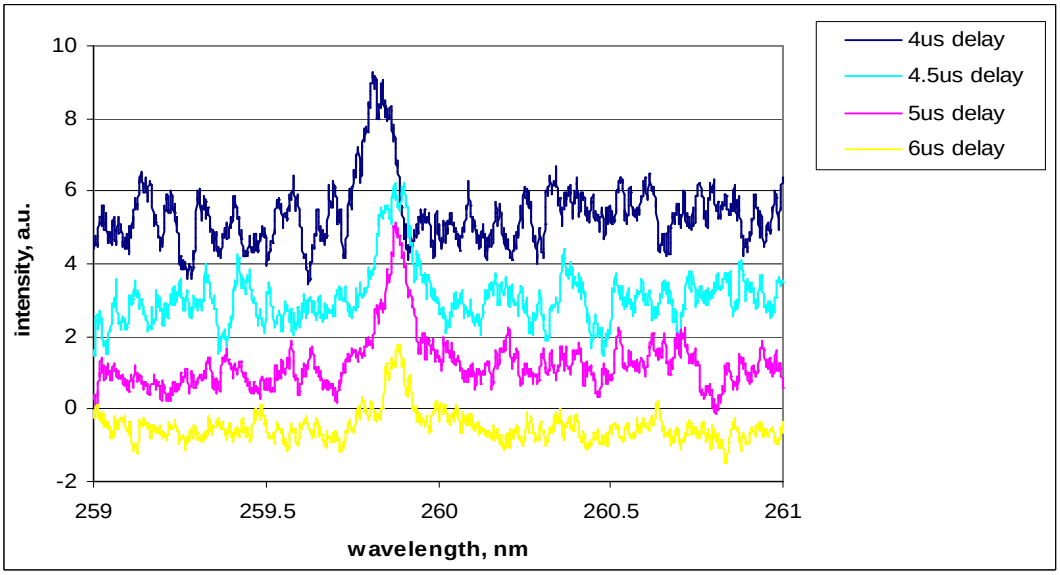

Figure 26. Sb Emission Peaks @ 259.9 nm, Different Time Delays, 100 ns gate width

Slit width 30 μm, higher laser energy

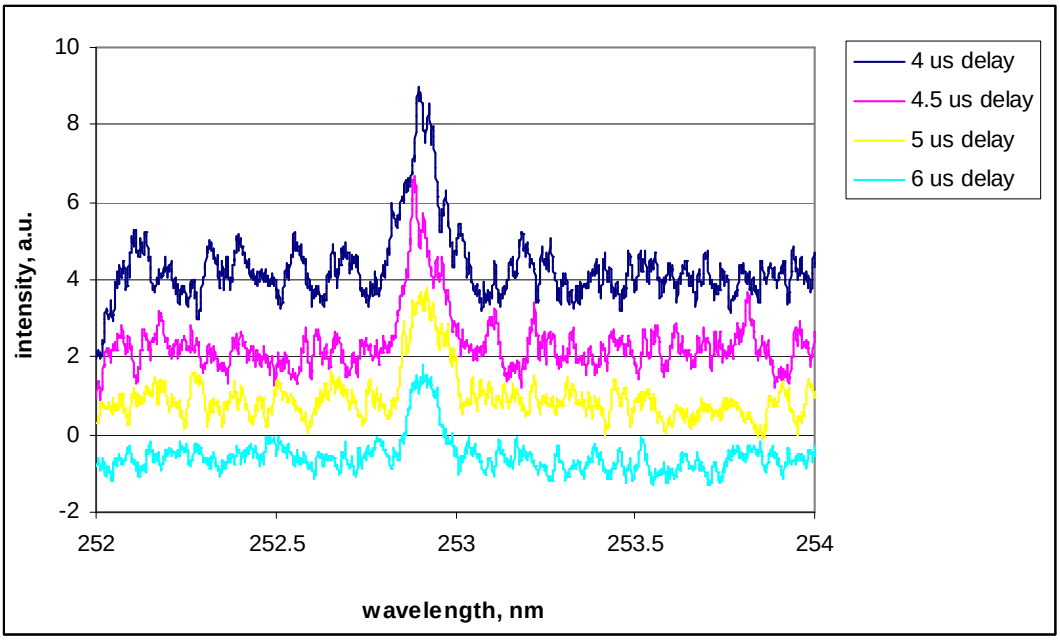

Figure 27. Sb Emission Peaks @ 252.9 nm, Different Time Delays, 100 ns gate width

Slit width 30 μm, higher laser energy

Figures 26 and 27 show emission peaks of Sb at different time delays with a gate width of 100 ns at the higher laser energy. The conditions were equivalent for both wavelengths.

6.2.1 Determination of Plasma Excitation Temperature for Sb

Plasma excitation temperatures were determined as a function of plasma decay time using peak emission intensity and peak area for Sb measurements at the two different wavelengths and laser energies. Tables 11 and 12 show peak emission intensities and areas corresponding to plasma decay times for Sb at 252.2 nm and 259.9 nm respectively at the lower laser energy.

time delay, us	intensity, a.u.	area
2	3.18	1986
3	2.01	484
4	1.40	136
5	1.18	43
6	0.96	56
7	0.68	97

Table 11. Sb Emission Peak Intensity/Area Versus Time Delay for 252-254 nm, lower laser energy

time delay, us	intensity, a.u.	area
2	4.35	2045
3	1.94	502
4	1.49	140
5	1.34	44
6	1.10	61
7	0.75	148

Table 12. Sb Emission Peak Intensity/Area Versus Time Delay for 259-261 nm, lower laser energy

The two wavelengths were used to determine the temperature of the plasma assuming that local thermodynamic equilibrium exists. These studies show that the calculated electron densities (N_e) satisfy the local thermodynamic equilibrium conditions in that: $N_e \geq 1.6 \times 10^{12} T^{1/2} (\Delta E)^3$, where T is temperature (K) and ΔE is the energy gap.[10] The ratio of the 259.9 nm line to the 252.9 nm line is calculated from the graphs in figure 28 and 29; tables 13 and 14 show the data for calculating the ratio and the plasma temperature. The ratio calculation is based on the following equation[26] :

$R = (I_1 * 1.25)/I_2$ for low laser energy

$R = I_1/I_2$ for high laser energy

I_1 = intensity at 259.9 nm

I_2 = intensity at 252.9 nm

The temperature calculation is based on the revised Boltzmann equation below using intensity ratio (or peak area) values from the equation above (the factor of 1.25 takes into account the different filter values used during the low laser energy measurements).

$$\mathbf{T = \Delta E/k * 1/ln\,[I_1 \lambda_1 g_2 A_2 / I_2 \lambda_2 g_1 A_1]}$$

$$\mathbf{\Delta E/k = 3451.7\ K}$$

$$\mathbf{g_1 A_1 = 64 \times 10^8\ s^{-1}}$$

$$\mathbf{g_2 A_2 = 56 \times 10^8\ s^{-1}}$$

$$\mathbf{\lambda_1 = 259.805\ nm}$$

$$\mathbf{\lambda_2 = 252.852\ nm}$$

259-261 nm	252-254 nm	ratio of 259:252	Plasma Temperature, K
4.35	3.18	1.71	8027
2.01	1.94	1.21	22681
1.49	1.40	1.33	19279
1.34	1.18	1.42	14152
1.10	0.96	1.43	13650
0.75	0.68	1.38	16075

Table 13. Plasma Temperature Calculations Using Peak Intensity at Lower Laser Energy

259-261 nm	252-254 nm	ratio of 259:252	Plasma Temperature, K
2045	1986	1.29	23640
502	484	1.30	22523
140	136	1.29	23686
44	43	1.28	24703
61	56	1.36	17066
148	97	1.91	6401

Table 14. Plasma Temperature Calculations Using Peak Area at Lower Laser Energy

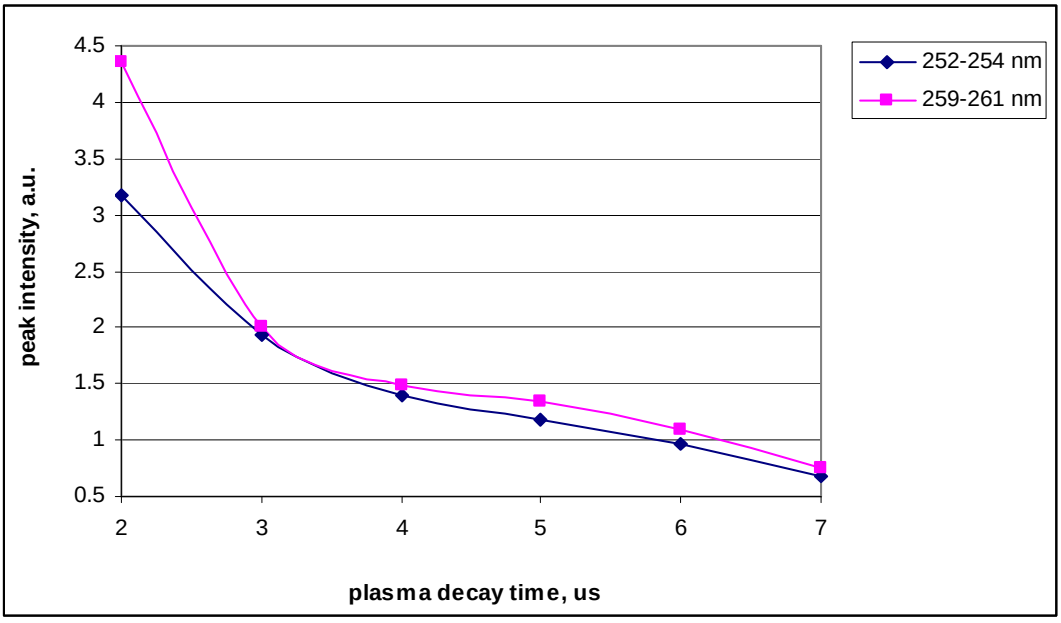

Figure 28. Sb Emission Peak Intensity Versus Plasma Decay Time at Low Laser Energy

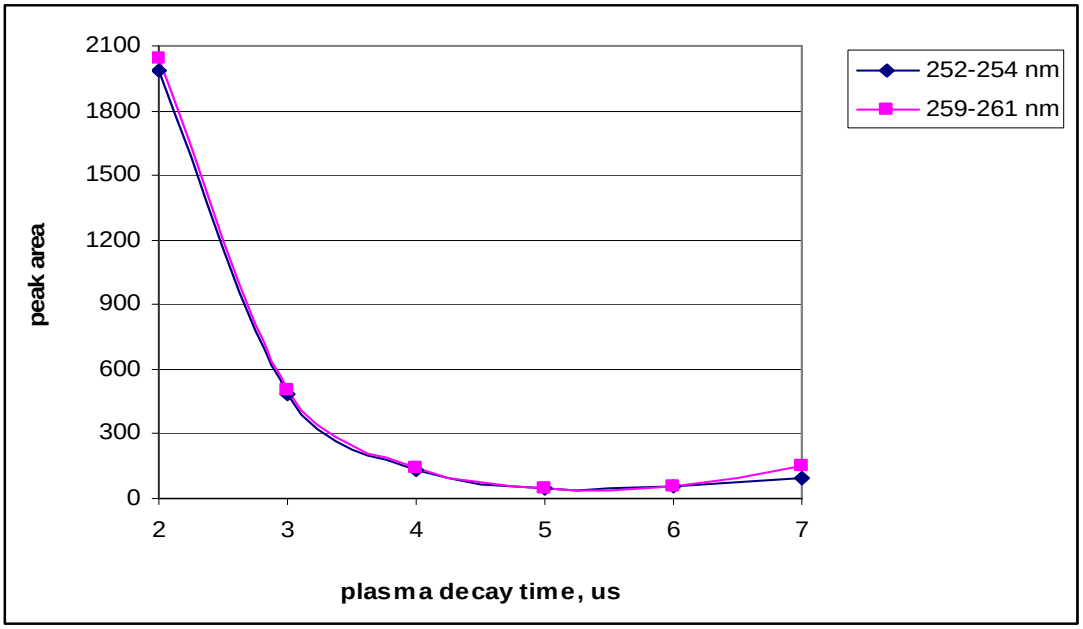

Figure 29. Sb Emission Peak Area Versus Plasma Decay Time at Low Laser Energy

Figures 30 and 31 show emission peak intensity/area versus plasma decay time using high laser energy; these figures are comparable to figures 28 and 29 at lower laser energy. Tables 15 and 16 provide the peak intensity/area and time delay data and table 17 provides the ratio and plasma temperature calculations.

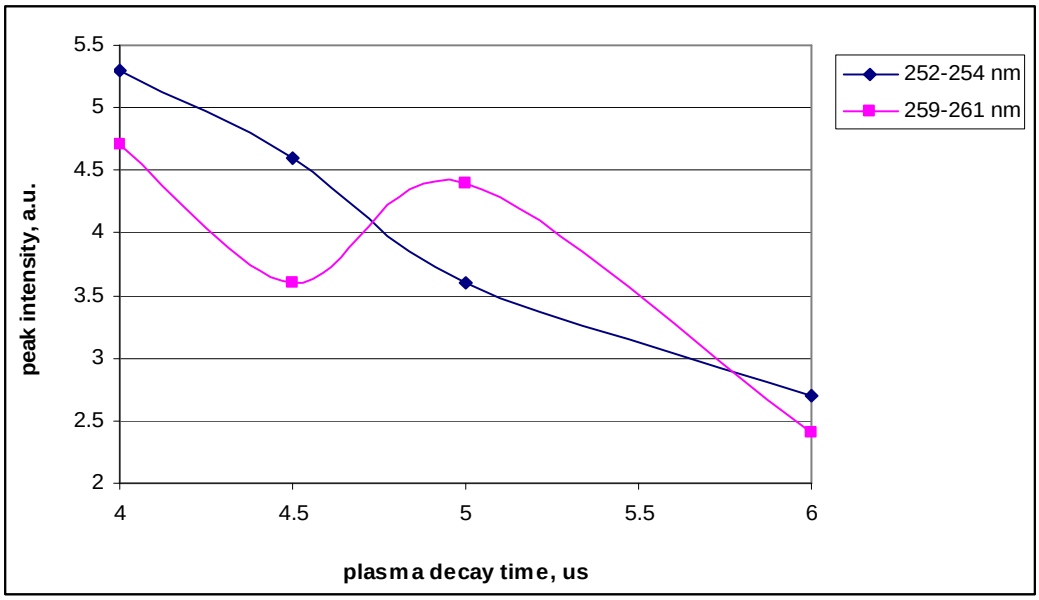

Figure 30. Sb Emission Peak Intensity Versus Plasma Decay Time at High Laser Energy

time delay, us	intensity, a.u.
4	5.3
4.5	4.6
5	3.6
6	2.7

Table 15. Sb Emission Peak Intensity And Time Delay for 252-254 nm, higher laser energy

time delay, us	intensity, a.u.
4	4.7
4.5	3.6
5	4.4
6	2.4

Table 16. Sb Emission Peak Intensity And Time Delay for 259-261 nm, higher laser energy

259-261 nm	252-254 nm	ratio of 259:252	Plasma Temperature, K
4.7	5.3	0.9	15236
3.6	4.6	0.8	9819
4.4	3.6	1.2	36616
2.4	2.7	0.9	15397

Table 17. Plasma Temperature Calculations Using Peak Intensity at High Laser Energy

6.2.2 Sb Calibration Curves

Calibration curves were generated for solutions of Sb at wavelengths of 252.9 nm and 259.9 nm. The calibration solution concentrations ranged from 1 ppm to 10 ppm with a blank solution of 0 ppm. Optimized instrument parameters were used from table 10 for both wavelengths. Figure 31 shows a calibration curve for Sb at 252.9 nm for a 252-254 nm wavelength range. The LOD for the calibration curve in figure 31 is 0.32 ppm. Figure 32 shows a calibration curve for Sb at 259.9 nm for a 259-261 nm wavelength range. The LOD for the calibration curve in figure 32 is 0.50 ppm. Figure 33 shows a calibration curve of Sb at a fixed wavelength of 252.9 nm with a LOD of 0.25 ppm. Figure 34 shows a calibration curve of Sb at a set wavelength of 259.9 nm with a LOD of 0.35 ppm. The conditions employed for figures 33 and 34 are outlined in table 10. Figures 35 and 36 show calibration curves of Sb with the averaging set at 1000. The wavelength is set at 252.9 nm in figure 35 and the LOD is 0.24 ppm. The wavelength is set at 259.9 nm in figure 36 and the LOD is 0.23 ppm. The instrument parameters for figures 35 and 36 are outlined in table 10. Figure 37 shows a calibration curve of Sb at 259.9 nm at higher laser energy. The conditions employed for figure 37 include a wavelength range of 259-261 nm, 5 μs time delay, 100 ns gate width, 30 μm slit width, averaging 10 and signal 10 mV/V. The LOD for the calibration curve in figure 37 is 0.34 ppm.

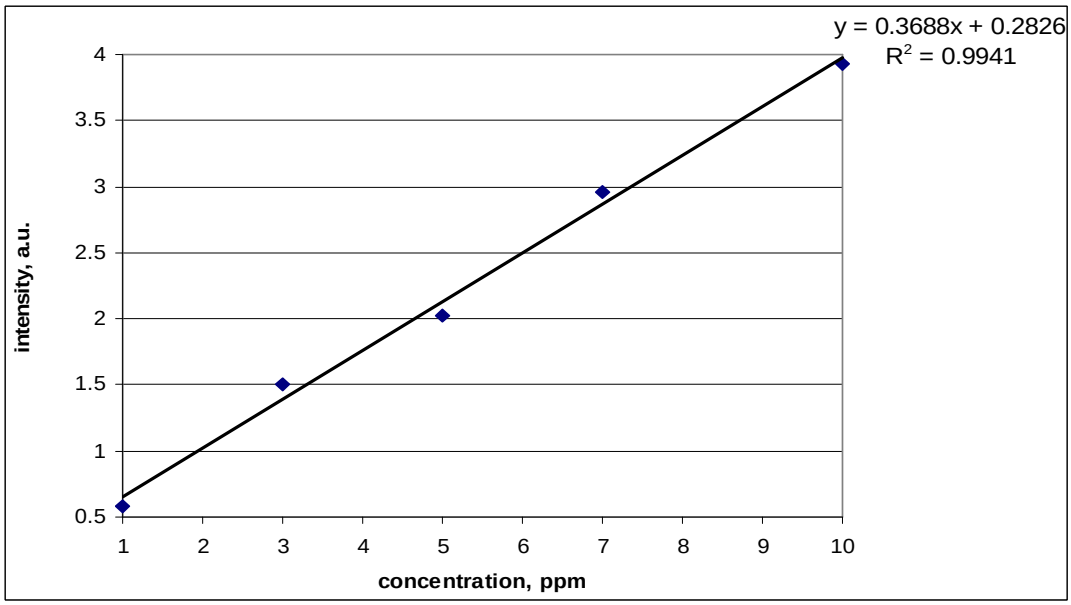

Figure 31. Sb Calibration Curve-1, 252.9 nm

Wavelength range 252-254 nm, LOD 0.32 ppm, time delay 2 µs, gate width 3 µs, slit width 40 µm

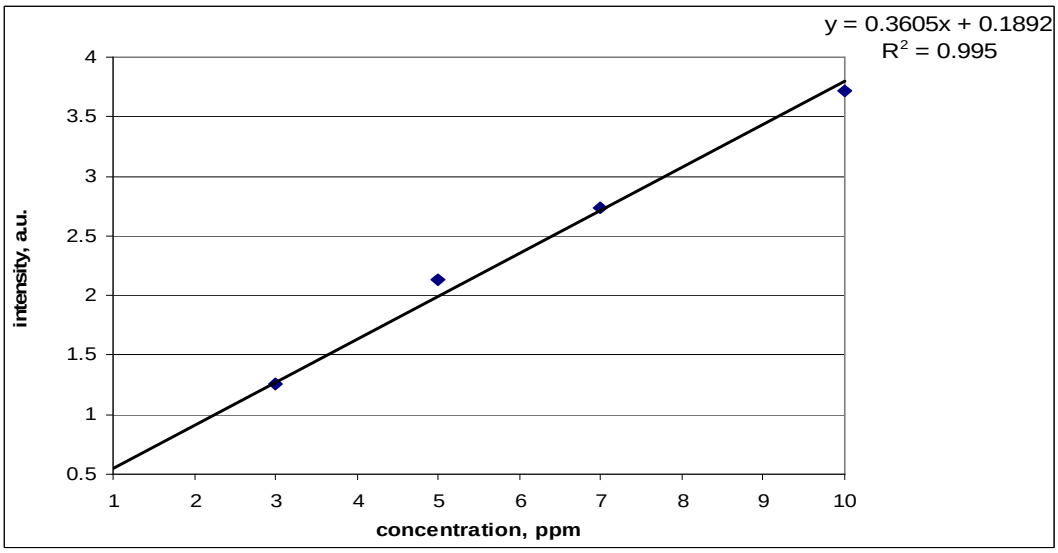

Figure 32. Sb Calibration Curve-1, 259.9 nm

Wavelength range 259-261 nm, LOD 0.50 ppm, time delay 2 µs, gate width 3 µs, slit width 40 µm

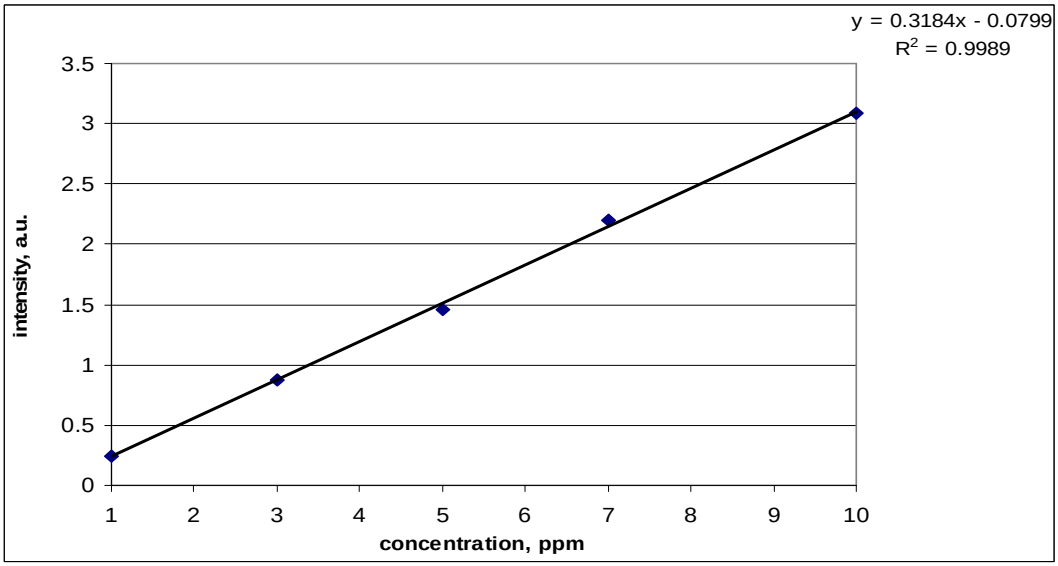

Figure 33. Sb Calibration Curve-2, 252.9 nm

Fixed wavelength 252.9 nm, LOD 0.25 ppm, time delay 2 µs, gate width 3 µs, slit width 40 µm

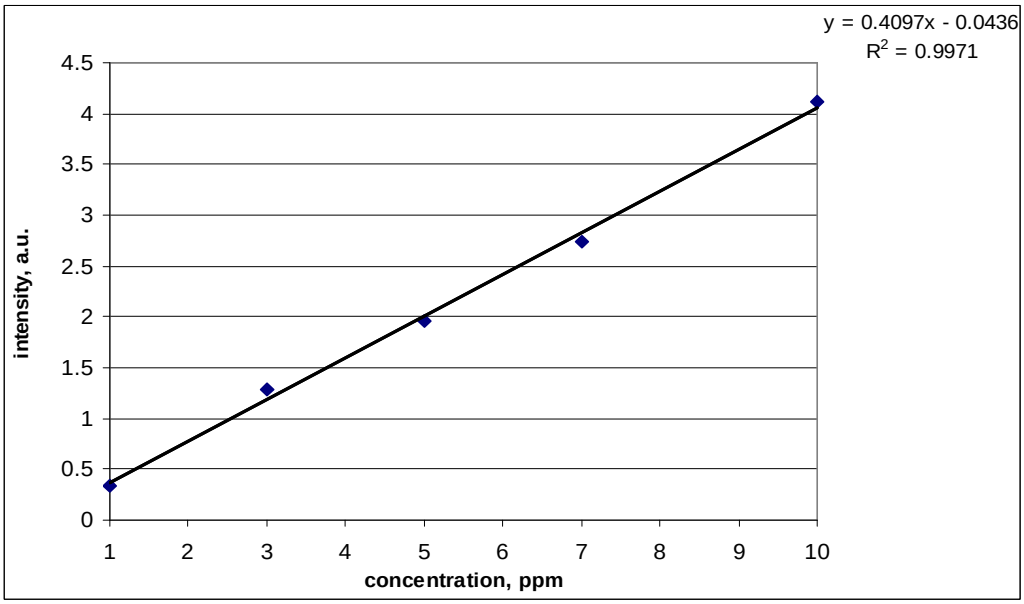

Figure 34. Sb Calibration Curve-2, 259.9 nm

Fixed wavelength 259.9 nm, LOD 0.35 ppm, time delay 2 µs, gate width 3 µs, slit width 40 µm

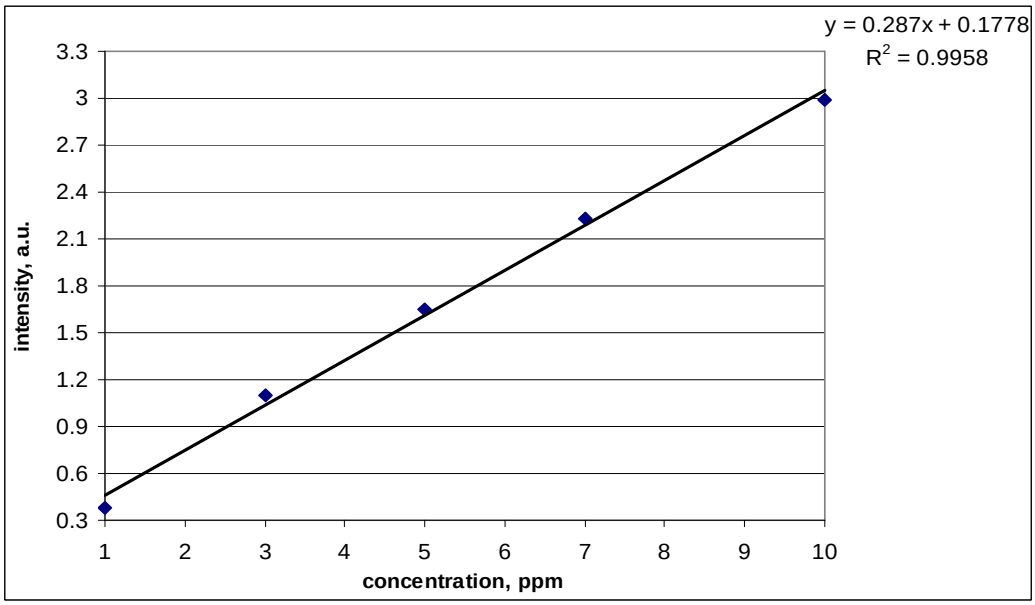

Figure 35. Sb Calibration Curve-3, 252.9 nm

Fixed wavelength 252.9 nm, LOD 0.24 ppm, time delay 2 µs, gate width 3 µs, slit width 40 µm, averaging 1000

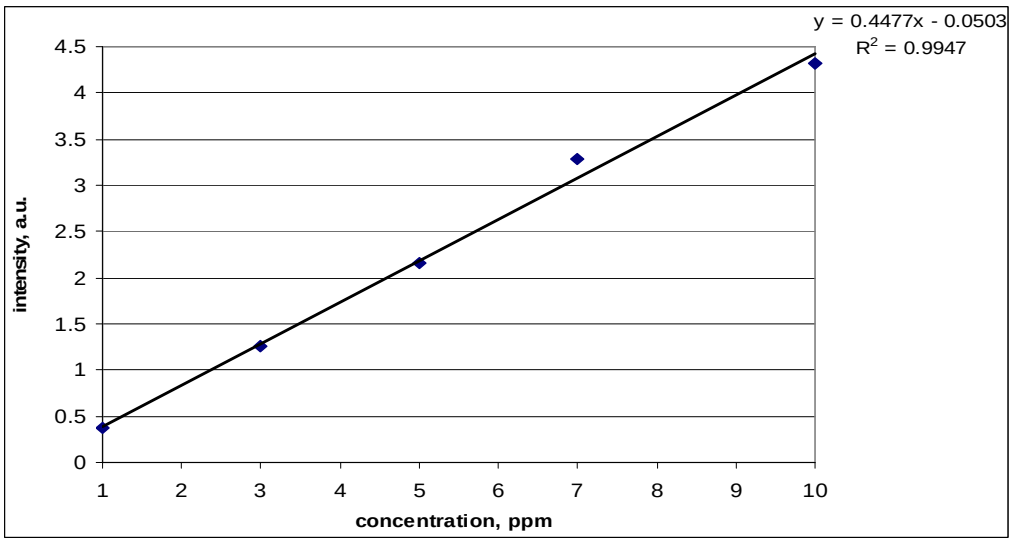

Figure 36. Sb Calibration Curve-3, 259.9 nm

Fixed wavelength 259.9 nm, LOD 0.23 ppm, time delay 2 µs, gate width 3 µs, slit width 40 µm, averaging 1000

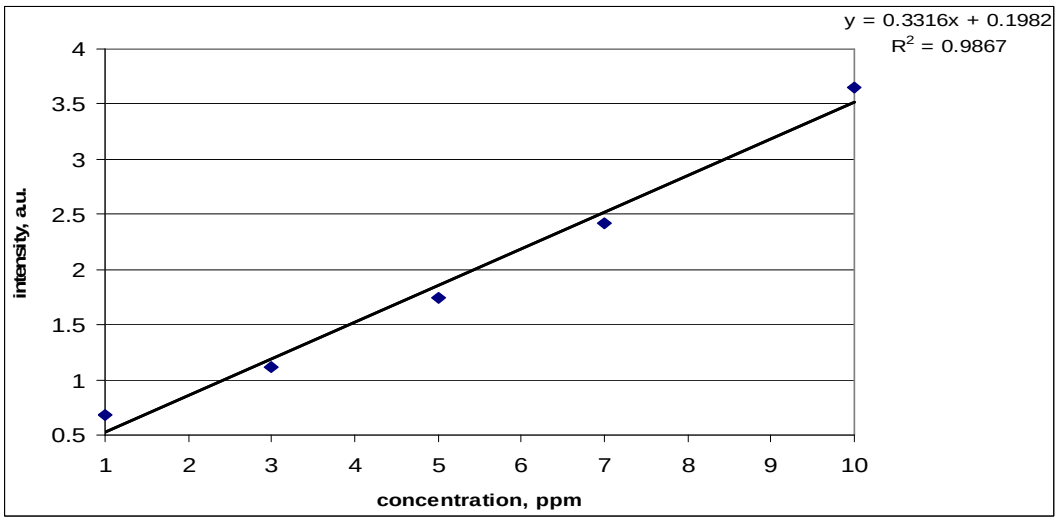

Figure 37. Sb Calibration Curve, 259.9 nm, Higher Laser Energy

Wavelength range 259-261 nm, 100 ns gate width, 5 µs time delay, 30 µm slit width, averaging 10, signal 10 mV/V, LOD 0.34 ppm

6.2.3 Discussion

Sb emission spectra were observed at wavelengths of 252.9 nm and 259.9 nm. The conditions employed during measurements were equal for the two different wavelengths as outlined in table 10. The maximum emission intensity resulted from measurements taken at 259.9 nm. Instrument parameters were adjusted according to learned characteristics of the plasma from hydrogen emission measurements. Sb emission spectra show changes in the life of the plasma in figures 22 and 23; the intensity and peak width decrease as time delays increase.

Sb calibration curves show a range of detection limits based on a fixed monochromator wavelength compared to a wavelength range and also a change in the instrumental averaging parameter. For lower laser energy, the LOD for 252.9 nm

measurements was the most sensitive when the wavelength was fixed at 252.9 nm with the averaging set at 1000; the LOD was 0.24 ppm. The LOD for 259.9 nm was very similar under the same conditions; the LOD was 0.23 ppm. The detection limits for the two different fixed wavelengths of 252.9 nm and 259.9 nm are similar in value and differ in value when the wavelength is set at a range. There's also a difference in the detection limit value when the averaging parameter is set at 10 versus 1000. The calibration curve generated at higher laser energy under a set wavelength range yields a LOD value of 0.34 ppm which is not lower than the value obtained at lower energy. LOD calculations were done using peak areas as opposed to peak intensities and the results were not comparable. The LOD calculated from peak areas ranged from 1.5-3.8 ppm. More research needs to be done on calibration curves at higher and lower laser energies as well as peak area versus peak intensity values for LOD.

The two different wavelengths of Sb were used in this work to determine the temperature of the plasma using the Boltzmann equation. Tables 13 and 14 show calculated plasma temperatures using peak intensities at the lower laser energy. The calculated plasma temperature range using peak intensities is 8027-22681 K. As the ratio of the two intensities decrease, the temperature increases. Similar calculations were done using the higher laser energy. The calculated plasma temperature range (9819-36616 K) using peak intensity at higher laser energy is higher, but comparable to the values obtained using peak intensity at lower laser energy. The results are as expected for calculated higher plasma temperatures using higher laser energy (peak intensity-based). The results are also comparable to other research showing the calculated plasma temperatures based on peak intensity. Table 18 provides information on calculated

plasma temperatures for this and other works for comparison. The results for detection limits of Sb using HG-LIBS are comparable to other works and this information is provided in table 20.

Plasma temperature, K	Reference
14000	Parigger et al[28]
11000	Parigger et al[29]
37000	Parigger et al[29]
10000-20000	Parigger et al[28]
5300-6625	Shaikh et al[31]
6401-36616	This work

Table 18. Plasma Temperature Comparisons

Method	Sb LOD, ppb	Reference
HPLC-HG-AFS	0.05-0.07	Bohari et al[24]
HG-ICP-AES	0.2	Sayago et al[32]
DHGN-ICP-OES	2.0	Rojas et al[19]
HG-AAS	0.2	Sturgeon et al[33]
DHG-AAS	0.02	Sun et al[34]
HG-LIBS	230	This work

Table 19. Sb Detection Limit Comparisons

6.3 SELENIUM EMISSION SPECTRA

Emission spectra of Se show a strong emission generated at a wavelength of 196.1 nm. During the measurements, the monochromator was set at a wavelength range of 195-197 nm with a scan rate of 1 nm/min. Figure 38 shows an emission peak of a 10 ppm solution of Se with background corrected peak intensity of 3.03 a.u. Table 20 provides the conditions of the measurements taken to obtain the maximum emission intensity of a 10 ppm solution of Se.

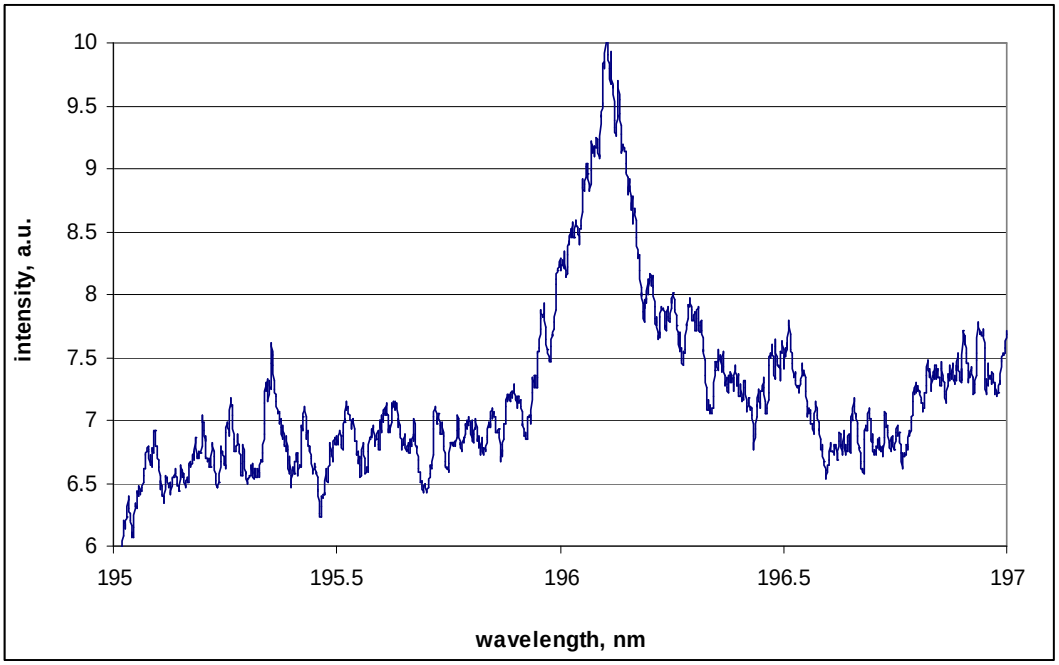

Figure 38. Se Emission Peak-1

Time delay 500 ns, gate width 3µs, averaging 10, slit width 40 µm, signal 10 mV/V

t_d, µs/ns	t_w, µs	Averaging (Avg)	Slit width, µm	Signal, mV/V	Max. intensity, a.u.
500 ns	3 µs	10	40	10	3.03
700 ns	3 µs	10	40	10	2.48
300 ns	3 µs	10	30	10	2.45
900 ns	3 µs	10	40	10	2.14

TABLE 20. Instrument Parameters and Conditions for Se Emission Peaks

Figure 39 shows Se emission spectra at different monochromator slit widths. Increasing the slit width allows more light to be detected including background emissions. Figure 40 shows Se spectra at different time delays with a gate width of 3 µs. Figures 41 and 42 show Se emission peaks at different time delays at a gate width of 100 ns. The instrument parameters are equivalent in figures 41 and 42 other than a 1.3 N.D. filter used in figure 42. Figure 43 shows emission peaks of Se at a higher laser energy. The slit width was 20 µm and the gate width was 100 ns; all other conditions were equivalent to those in table 20.

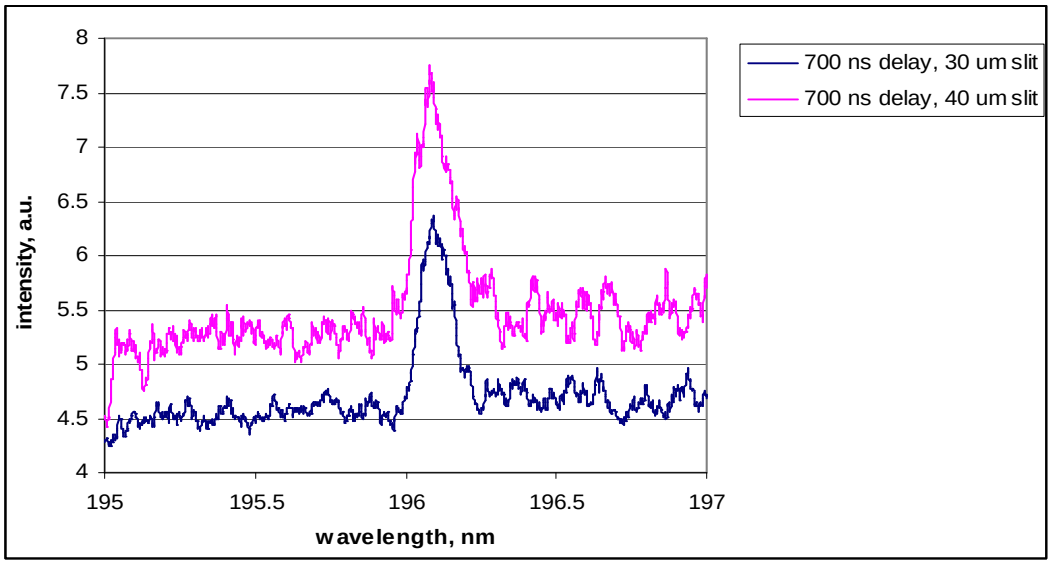

Figure 39. Se Emission Peaks at Different Slit Widths

Gate width 3 μs, averaging 10, signal 10 mV/V

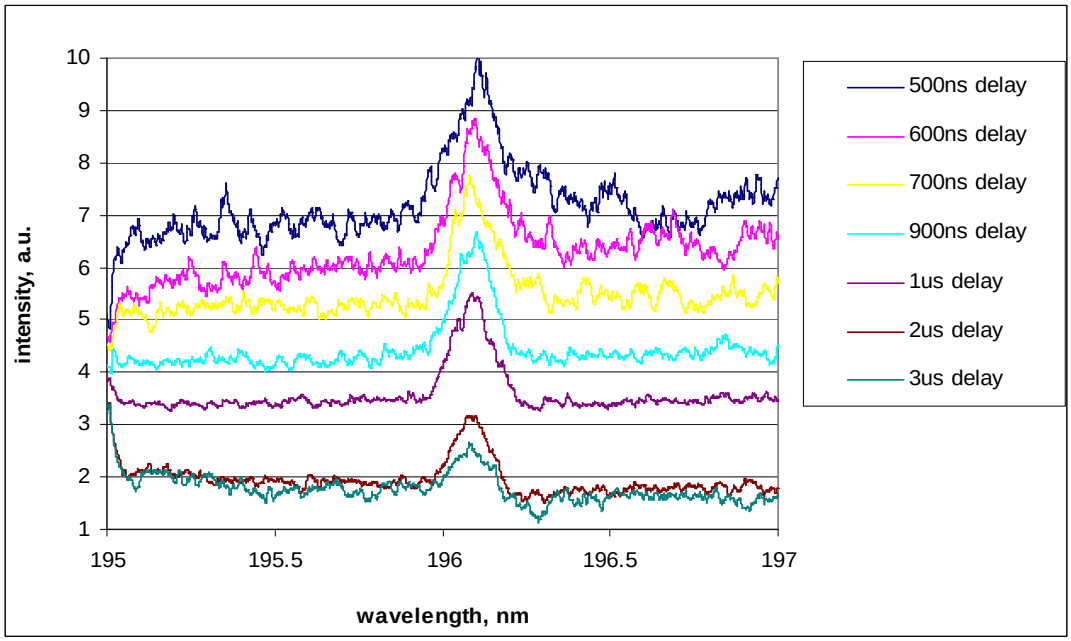

Figure 40. Se Emission Peaks at Different Time Delays-1

Gate width 3 μs, averaging 10, signal 10 mV/V, slit width 40 μm

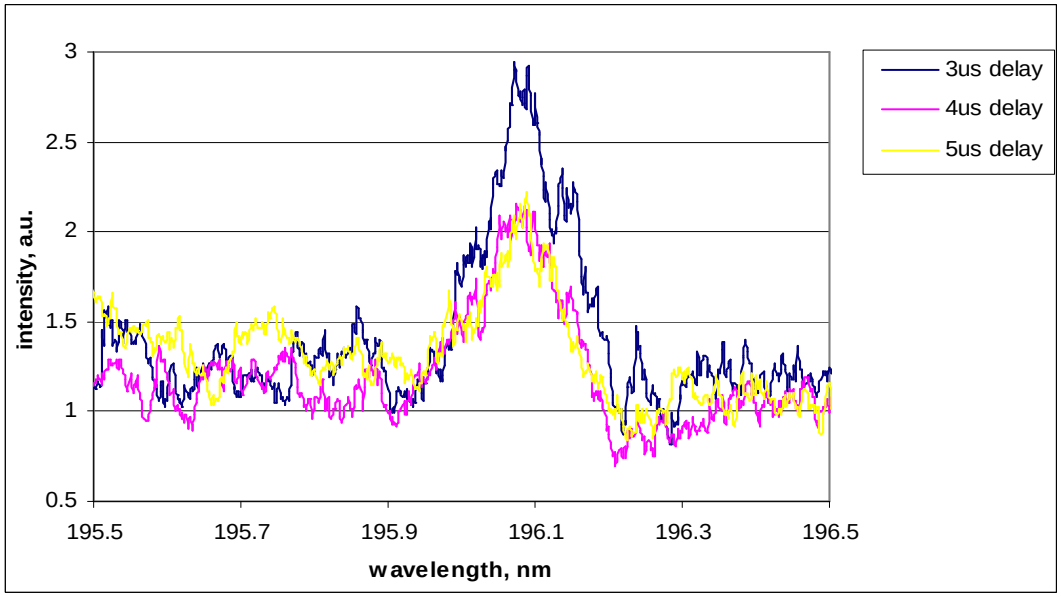

Figure 41. Se Emission Peaks at Different Time Delays-2

Gate width 100 ns

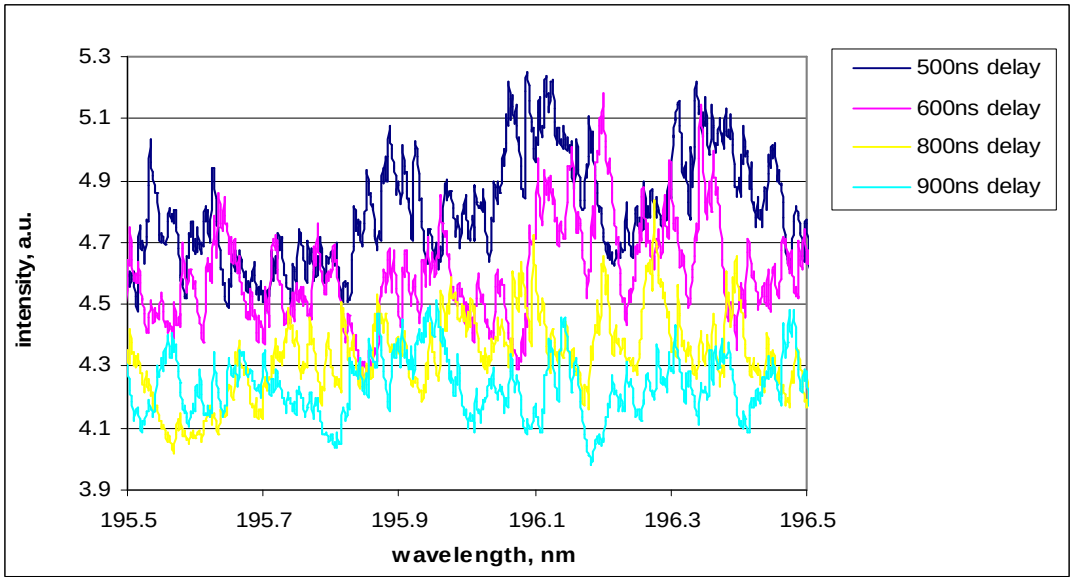

Figure 42. Se Emission Peaks at Different Time Delays-3

Gate width 100 ns, 1.3 N.D. filter

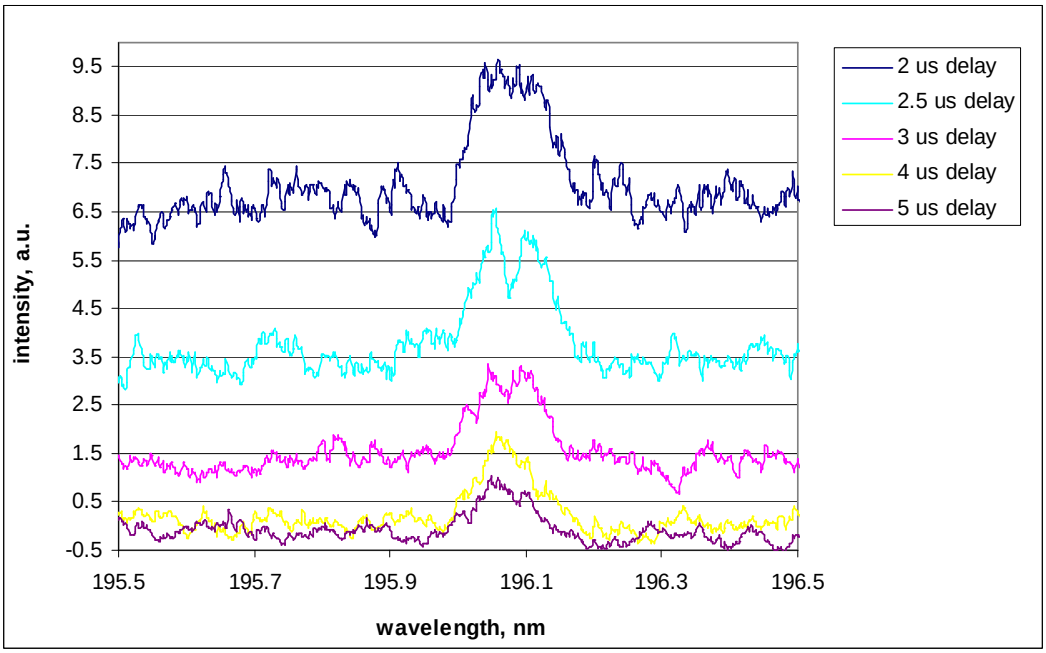

Figure 43. Se Emission Peaks at Different Time Delays-4

Higher laser energy, slit width 20 µm, gate width 100 ns

6.3.1 Se Calibration Curves

Calibration curves were generated for Se solutions ranging from 0 ppm to 10 ppm. The limit of detection was calculated in this work from the calibration curve using the following:

LOD = (3*σ)/m

σ = the standard deviation, SD, of the blank solution (16 assays)

m = the slope of the calibration curve

LOD is expressed in units of concentration

Figure 44 shows a calibration curve of Se emission peaks that are representative of the maximum emission intensity parameters outlined in table 20 for a 500 ns time delay; the LOD is 0.80 ppm. Figure 45 is a calibration curve of Se using the parameters in table 20 for a 300 ns time delay at a wavelength of 196.1 nm; the LOD is 1.4 ppm and the monochromator was set at a fixed wavelength of 196.1 nm. Figure 46 shows a calibration curve of Se emission peaks under the same conditions as the calibration curve in figure 45 with the averaging set at 1000 instead of 10; the LOD for this calibration is 0.58 ppm. Figure 47 shows a calibration curve from data obtained using higher laser energy and the LOD is 0.41 ppm. The conditions for figure 47 are different than those in figures 44-46; the time delay is 4 μs, the gate width is 100 ns, the averaging is 10, the signal is 10 mV/V, the wavelength range is 195-197 nm and the slit width is 30 μm.

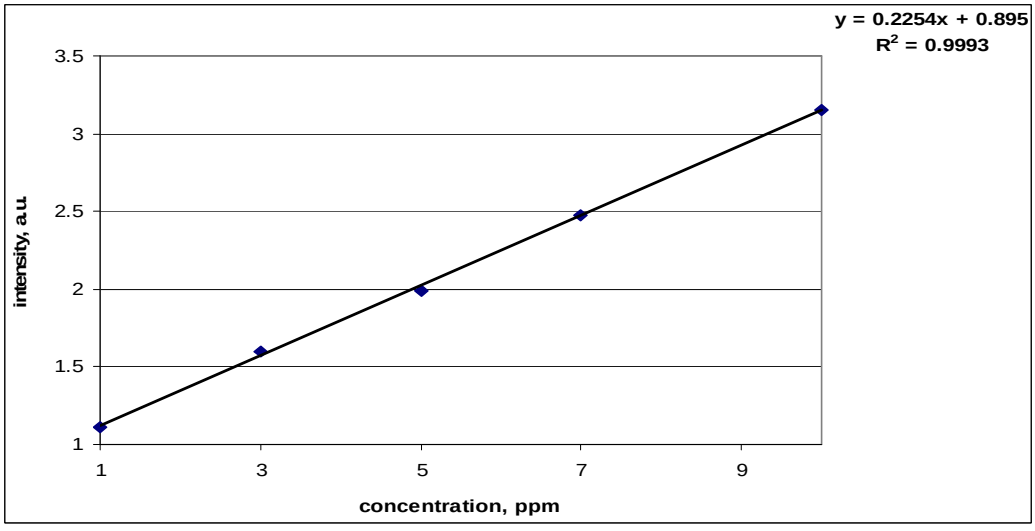

Figure 44. Se Calibration Curve-1

Peak intensity calibration curve: LOD 0.80 ppm, Time delay 500 ns, gate width 3μs, averaging 10, slit width 40 μm, signal 10 mV/V, 195-197 nm wavelength range

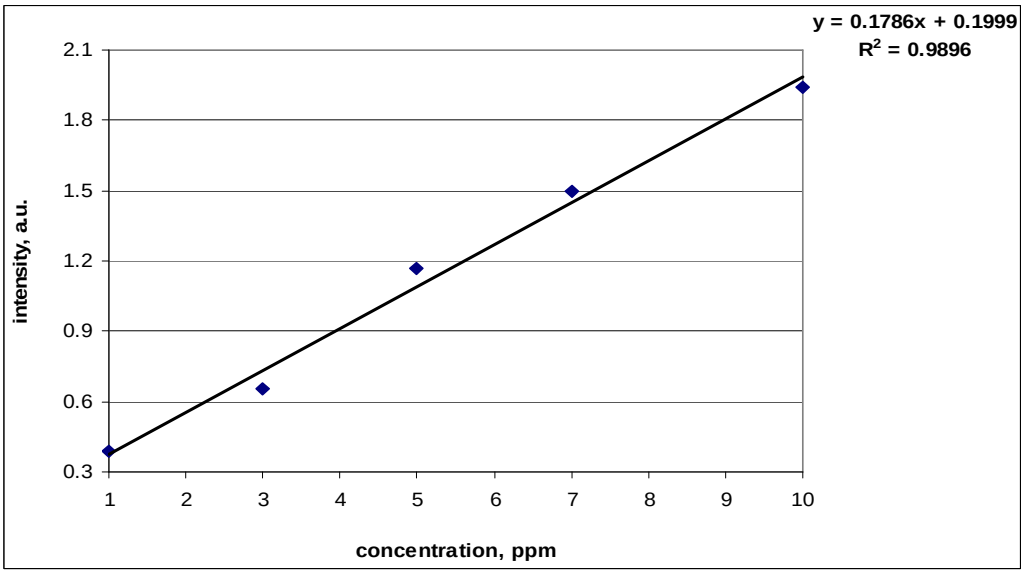

Figure 45. Se Calibration Curve-2

Peak intensity calibration curve: LOD 1.4 ppm, Time delay 300 ns, gate width 3µs, averaging 10, slit width 30 µm, signal 10 mV/V, 196.1 nm fixed wavelength

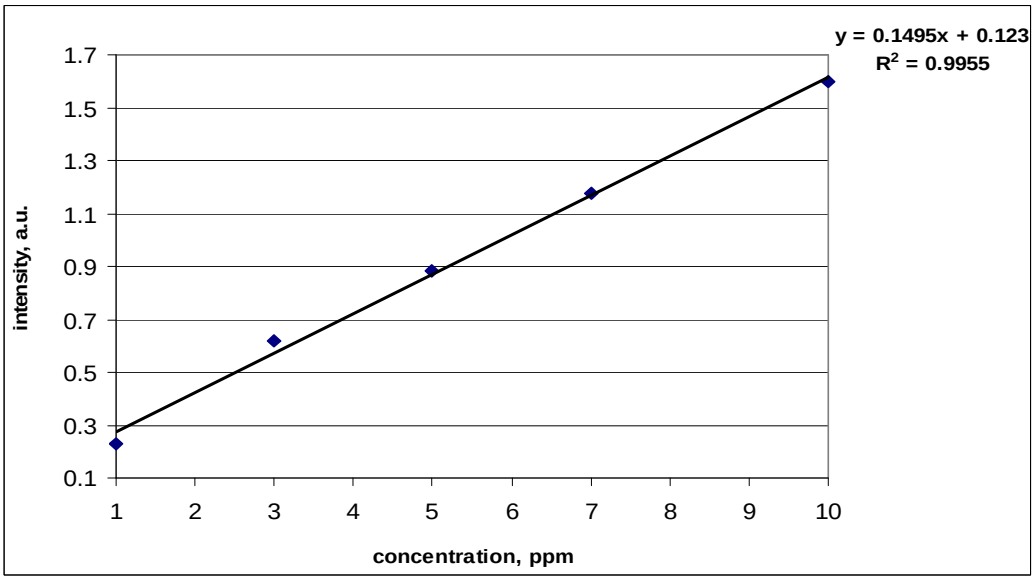

Figure 46. Se Calibration Curve-3

Peak intensity calibration curve: LOD 0.58 ppm, Time delay 300 ns, gate width 3µs, averaging 1000, slit width 30 µm, signal 10 mV/V, 196.1 nm fixed wavelength

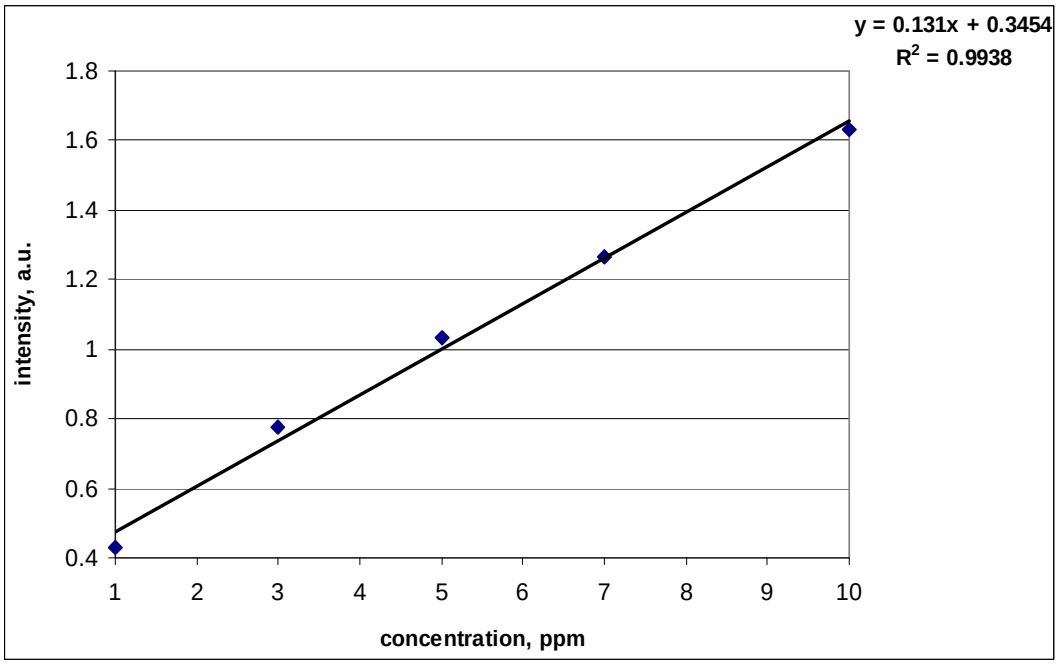

Figure 47. Se Calibration Curve-4

Peak intensity calibration curve higher laser energy: LOD 0.41 ppm, Time delay 4 μs, gate width 100 ns, averaging 10, slit width 30 μm, signal 10 mV/V, 195-197 nm wavelength range

6.3.2 Discussion

The data shows that Se atoms can be detected at ppm levels at a wavelength of 196.1 nm during HG-LIBS measurements. Instrument parameters were adjusted to obtain the maximum emission intensity to generate a sharp, well defined peak with minimal background. Adjusting parameters such as time delay and gate width affected the intensity of the peak due to the time dependent changes in the plasma. Table 20 provides data that shows a decrease in peak intensity with an increase in time delay; a time delay of 500 ns resulted in a peak with an intensity of 3.03 a.u. and a time delay of 900 ns, resulted in an intensity of 2.14 a.u. Figure 39 shows the changes in emission

peaks with different monochromator slit widths. As the slit width increases, the emission peaks are broader and the background increases due to increased light reaching the detector. Detecting emissions at different slit widths is one of the tools in adjusting parameters to achieve the best sensitivity and signal to noise. A slit width of 40 μm was chosen as the best setting based on the data in figure 39 showing that there is a higher signal even though there is high background.

Figures 40, 41, and 42 show peaks of different time delays with the same gate width. The changes in the peak emissions indicate that the temperature of the plasma decreases as the time delay increases. The gate width of 100 ns resulted in peaks that were not as clear in figure 42 when compared to those in figure 41. Also, the background was very high for the peaks at small time delays in figure 42 and this was not the case for the peaks in figure 41. The differences in the two figures are due to the significant changes in the plasma over time. Figure 43 is comparable to figures 41 and 42; the peaks are generated from the higher laser energy. A slit width of 20 μm was used in the measurement of peaks for figure 43. The time delay range of 2 μs to 5 μs was used during measurements taken at higher laser energy as opposed to a time delay range of 3 μs to 5 μs at lower energy. The time delay ranges differ due to the slit width differences which determine how much light reaches the detector.

Once the parameters were optimized, a calibration curve was generated using solutions of Se ranging from 0-10 ppm. There was a linear response in concentration vs. intensity; figures 44-47 are calibration curves showing the increase in intensity with an increase in concentration. The LOD for Se measurements using the HG-LIBS technique range from 0.41 ppm to 1.4 ppm. The instrument parameters outlined in table 20 for a

500 ns time delay show a LOD of 0.80 ppm for a 10 ppm solution of Se. The results of this work using lower laser energy show that the LOD is most sensitive at a fixed wavelength instead of scanning a wavelength range and with the averaging set at 1000 instead of 10; the value is 0.58 ppm. The results using higher laser energy yield a lower LOD of 0.41 ppm at a wavelength range of 195-197 nm. As discussed in Sb analysis, peak area values were used for calculating the detection limit and the results were not comparable to those using peak intensity values. The calculated LOD using peak areas was in the range of 3.5-4.7 ppm. More research needs to be done on the higher versus lower laser energy for a better comparison of the two methods of analysis. Table 21 shows comparisons LOD values for Se and other elements using hydride generation.

Additives such as methanol and ethanol were added to solutions of Se for enhancement effects. Although it has reported that these additives can enhance the sensitivity, there was no observed enhancement on sensitivity and the additive did not show linearity in its addition.

Method	**LOD, ppb**	**Element**	**Reference**
HG-LIF	0.00009	Se	Pacquette et al[12]
HG-ICP-AES	30	Se	Saisho et al[35]
DHGN-ICP-AES	0.1	Se	Rojas et al[19]
HG-AFS	0.2	Se	Gomez-Ariza et al[36]
HG-LIBS	410	Se	This work

Table 21. Comparison of HG-LIBS LOD Values

6.4 CONCLUSION

The data in this work show that hydride generation coupled to laser induced breakdown spectroscopy is a good technique for performing trace elemental analysis and plasma diagnostics. Because the hydrogen peak is well isolated and has high intensity, HG-LIBS of hydrogen allowed the use of Stark Broadening of the H_α line to determine electron density of the plasma. FWHM data was calculated from emission peaks of hydrogen at a 100 ns gate width under optimized instrument parameters. The FWHM values were plotted against plasma decay time to show the decrease in peak width (electron density) as the time delay increased. Peak broadening of hydrogen emission peaks corresponded to electron density. Graphs of hydrogen emission peaks at a gate width of 100 ns and different time delays showed the peaks become less broad and less intense as the time delay increased. Se and Sb data showed the same peak broadening due to electron density of the plasma.

Plasma temperatures were determined for Sb analysis using the Boltzmann equation. Sb was measured at two different wavelengths and the theory of local thermodynamic equilibrium was applied to allow plasma temperature calculations based on the Boltzmann equation. The results show the plasma temperature to range from 6401-36616K. The temperature range is comparable to many different works and shows that the early plasma is very hot and cools as the time delay increases.

Two different laser energies were used to measure emission peaks of elements to determine if the sensitivity of the method changes. The results show that the detection limit using HG-LIBS is in the low ppm range for both high and low laser energy and can

be made more sensitive with additional work in plasma diagnostics. Se results show detection limits ranging from 0.41-1.4 ppm and Sb detection limits range from 0.23-0.50 ppm. The use of higher laser energy increased the detection limit for both elements. The LOD results for both Sb and Se are comparable to other methods and techniques using hydride generation.

6.5 FUTURE WORK

Future work on this research includes speciation of the analyte as well as separation techniques by HPLC methods. Also, enhancement of the analyte in solution using an organic additive such as ethanol should be performed to determine if the sensitivity is increased. Further measurements at two different laser energies should be done for a comparison analysis. In addition, the use of an array detector should be explored to increase the signal to noise ratio and improve the LOD. Finally, hydride generation should be combined with laser induced fluorescence for better sensitivity and selectivity.

CHAPTER 7: REFERENCES

[1] Skoog, D.; Holler, J.; Crouch, S. (2007). *Principles of Instrumental Analysis Sixth Edition*. Thomson Brooks/Cole.

[2] Robinson, J. (1995). *Undergraduate Instrumental Analysis Fifth Edition*. New York: Marcel Dekker.

[3] Winefordner, J.D.; Gornushkin, I.B.; Pappas, D.; Matveev, O.I.; Smith, B.W. *J. Anal. Spectrom.* **2000**, 15, 1161-1189.

[4] Manning, T.; Grow, W. *The Chemical Educator*. **1997**, 2, 2-19.

[5] Hieftje, G.M. *Fresnius J. Anal. Chem.* **1990**, 337, 528-537.

[6] De Regt, J.M.; de Groote, F.P.J.; van der Mullen, J.A.M.; Schram, D.C. *Spectrochimica Acta Part B,* **1996**, 51, 1371-1383.

[7] Rauschenbach; Lazic, V.; Pavlov, S.G.; Hubers, H.W.; Jessberger, E.K. *Spectrochimica Acta Part B,* **2008**, 63, 1205-1215.

[8] Sherbini, A.M.; Hegazy, H.; Sherbini, Th.M. *Spectrochimica Acta Part B,* **2006**, 61, 532-539.

[9] Oks, E.; Derevianko, A.; Ispolatov, Ya. *J. Quant. Spectrosc. Radiat. Transfer*, **2005**, 54, 307-315.

[10] AI, HUA, LIU, *J. Plasma Physics*. **2007**, 73, part 2, 231-239.

[11] Burakov, V.S.; Tarasenko, N.V.; Kononov, V.A.; Vasilev, N.N.; Isakov, S.N. *Spectrochimica Acta Part B:* **2009**, 64, 141-146.

[12] Pacquette, H.L.; Elwood, S.A.; Ezer, M.; Simeonsson, J.B. *J. Anal. At. Spectrom.* **2001**, 16, 152-158.

[13] Wei, L.; Gupta, P.; Hernandez, R.; Farhat, F. *Microchemical Journal* **1999**, 62, 83-98.

[14] Marchante-Gayon, J.M.; Feldmann, I.; Thomas, C.; Jakubowski, N. *J. Anal. At. Spectrom*. **2001**, 16, 457-463.

[15] Munozolivas, R.; Quetel, C.R.; Donard, F.X. *J. Anal. At. Spectrom*. **1995**, 10, 865-870.

[16] Cheng, E.A.P.; Fraser, R.D.; Eden J. G. *Applied Spectroscopy*, **1991**, 45, 949.

[17] ^ "Dietary Supplement Fact Sheet: Selenium". National Institutes of Health; Office of Dietary Supplements. http://ods.od.nih.gov/factsheets/selenium.asp. Retrieved 2009-08-25.

[18] Zhang, Y.; Adeloju, S.B. *Talanta*, **2008**, 76, 724-730.

[19] Rojas, I.; Murillo, M.; Carrion, N. *Anal. Bioanal. Chem.* **2003**, 376, 110-117.

[20] Madrakian, T.; Bozorgzadeh, E. *Journal of Hazardous Materials*. **2009**, 170, 809-813.

[21] Ulrich, N. *Anal. Chim. Acta*. **1998**, 359, 245-253.

[22] Filella, M.; Belzile, N.; Lett, M. *Earth Science Reviews*. **2007**, 80, 195-217.

[23] Shotyk, W.; Krachler, M. *J. Environ. Monit.* **2009**, 11, 1747-1753.

[24] Bohari, Y.; Astruc, A.; Astruc, M.; Cloud, J. *J. Anal. At. Spectrom*. **2001**, 16, 774-778.

[25] Qiu, P.; Ai, C.; Lin, L.; Wu, J.; Ye, F. *Microchemical Journal*. **2007**, 87, 1-5.

[26] Kepple, P.; Griem, H.R. *Phys. Rev.* **1968**, 173, 317-325.

[27] Simeonsson, J.B.; Miziolek, A.W. *Applied Optics*. **1993**, 32, 939-947.

[28] Parigger, C.G; Dackman, M.; Hornkohl, J.O. *Applied Optics*. **2008**, 47, G1-G6.

[29] Parriger, C.G.; Plemmons, D.H.; Oks, E. *Applied Optics*. **2003**, 42, 5992-6000.

[30] Parigger, C.G.; Oks, E. *International Journal of Spectroscopy*. **2010**, 1-4.

[31] Shaikh, N.M.; Rashid, B.; Hafeez, S.; Jamil, Y.; Baig, M.A. *J. of Physics D: Applied Physics*. **2006**, 39, 1384-1391.

[32] Sayago, A.; Beltran, R.; Gomez-Ariz, J.L. *J. Anal. Spectrom.* **2000**. 15, 423-428.

[33] Sturgeon, R.E.; Willie, S.N.; Berman, S.S. *Anal.Chem.* **1985**, 57, 2311-2314.

[34] Sun, H.; Ha, J.; Sun, J.; Zhang, D.; Yang, L. *Anal.Bioanal. Chem.* **2002**, 374, 526-529.

[35] Saisho, H.; Fujimura, Y. *J. Analytical Sciences.* **1990**. 6, 619.

[36] Gomez-Ariza, J.L.; Sanchez-Rodas, D.; Morales, E.; Herrgott, O.; Marr, I.L. *Applied Organometallic Chemistry* **1999**, 13, 783-787.